A Seismic Hazard Model for Sub-Saharan Africa

Technical Report

PILOT PROJECT

VERSION 1.0.0

September, 2016

V. Poggi, R.J. Durrheim,
G. Mavonga Tuluka, M. Pagani,
G. Weatherill, J. Garcia,
A. Nyblade

GEM
GLOBAL EARTHQUAKE MODEL
working together to assess risk

A Seismic Hazard Model for Sub-Saharan Africa

globalquakemodel.org

USAID
FROM THE AMERICAN PEOPLE

This study is made possible by the generous support of the American people through the United States Agency for International Development (USAID). The contents are the responsibility of GEM and do not necessarily reflect the views of USAID or the United States Government.

Authors

V. Poggi[1], R. Durrheim[2], G. Mavonga Tuluka[3], M. Pagani[1],
G. Weatherill[1], J. Garcia[1], A. Nyblade[4]

[1] GEM Foundation, Pavia, Italy
[2] University of the Witwatersrand, Johannesburg, South Africa
[3] Goma Volcanic Observatory, DR Congo
[4] Penn State University, USA

Citation

Please cite this document as:

A Seismic Hazard Model for Sub-Saharan Africa

GEM Technical Report, Pavia, September 2016, DOI: 10.13117/GEM.REG.TR2016.01

Abstract

The East African Rift System (EARS) is the major active tectonic feature of the Sub-Saharan Africa (SSA) region. Although the seismicity level of such a divergent plate boundary can be described as moderate, several earthquakes have been reported in historical times causing a non-negligible level of damage, albeit mostly due to the high vulnerability of the local buildings and structures. Formulation and enforcement of national seismic codes is therefore an essential future risk mitigation strategy. Nonetheless, a reliable risk assessment cannot be done without the calibration of an updated seismic hazard model for the region.

Unfortunately, the major issue in assessing seismic hazard in Sub-Saharan Africa is the lack of basic information needed to construct source and ground motion models. The historical earthquake record is largely incomplete, while instrumental catalogue is complete down to sufficient magnitude only for a relatively short time span. In addition, mapping of seimogenically active faults is still an on-going program. Recent studies have identified major seismogenic lineaments, but there is substantial lack of kinematic information for intermediate-to-small scale tectonic features, information that is essential for the proper calibration of earthquake recurrence models.

In this study, we propose a new probabilistic seismic hazard model for the Sub-Saharan Africa region based on distributed seismicity. The model has been calibrated on the most recent and up to date information available from scientific literature, global bulletins and local earthquake catalogues, such as those from the partner AfricaArray project. In this report we describe in detail all working assumptions, main processing steps, data analyses and interpretations used for the model setup. OpenQuake input files for hazard computation are made openly available though GEM platform.

Keywords: East African Rift System, PSHA, Earthquake Catalogue, AfricaArray

Contents

1. Introduction

1.1 Seismic Risk in Central Africa

Earthquakes pose a significant risk in tectonically-active parts of sub-Saharan Africa more particularly in the *East African Rift System*, especially as cities grow and many buildings are constructed without taking potential ground shaking into account. While most earthquakes occur near plate boundaries, it must be noted that a damaging earthquake can occur anywhere, for example, in Guinea in 1983. A low rate of seismicity does not mean that the maximum possible size of an earthquake is small, just that earthquakes are less frequent. Furthermore, even a moderate-sized earthquake can prove disastrous should it occur near a city with many vulnerable buildings, as happened when an Mw 5.7 earthquake struck Agadir, Morocco in 1960, causing some 15,000 deaths. The epicentre of the 2008 Mw 5.9 Lac Kivu earthquake was about 20 km from the city of Bukavu in the DRC (population 250,000), and can be regarded as a "near miss".

The mitigation of earthquake risk in Africa requires coordinated action on several fronts. Firstly, seismic hazard assessments should be improved by maintaining and expanding seismic monitoring networks, supplementing historical and paleoseismic catalogues, and mapping active faults and the near-surface. Secondly, building codes should be formulated and enforced, and vulnerable existing buildings and infrastructure reinforced to prevent serious damage or collapse when subjected to strong shaking. Lastly, disaster management agencies, emergency first responders, and the general public should be trained to act effectively and sensibly during an earthquake, and equipped to deal with the aftermath. National efforts to assess seismic hazard are reviewed by Worku (2014). The Kenyan seismic code was issued in 1973 by the Kenyan Ministry of Works and uses the Modified Mercalli intensity (MMI) scale to map the seismic hazard of the country (MWK, 1973). The country was divided into four seismic zones: Zone V, VI, VII and VIII–IX. The building design code of Ethiopia was first introduced in 1978. Its seismic provisions have been revised twice since then. The first

revision took place in 1983. The current version, the Ethiopian Building Code Standard EBCS 8: 1995, provides a seismic hazard map based on a 100-year return period (MWUD, 1995). The seismic code of Uganda, US 319: 2003 was issued by the Uganda National Bureau of Standards in 2003 (UNBS, 2003). Three seismic zones were defined.

1.2 The AfricaArray Project

A significant impediment to the assessment of seismic hazard and risk in earthquake-prone areas of sub-Saharan Africa is the lack of high-quality seismic data from local and regional networks. The AfricaArray seismic network was launched in 2005 with a handful of stations in eastern and southern Africa. It is a research and capacity-building network established by Witwatersrand and Penn State universities and the South African Council for Geoscience. Over the past decade the AfricaArray "backbone" network has expanded to include 51 permanent stations in 19 countries as well as several temporary deployments. These data may have the potential to improve greatly the seismicity catalogues for much of Africa. The Global Earthquake Model (GEM) Foundation was launched in 2009 with the vision of promoting the collaborative development of tools and models for earthquake hazard and risk assessment.

In this report, we illustrate part of the activities completed within USAID-funded pilot project, where we seek to gain knowledge and build capacity to mitigate and reduce seismic risk in regions affected by earthquakes in sub-Saharan Africa associated with the East African Rift System by combining the expertise, technologies and infrastructure developed by AfricaArray. The first phase, which we report on here, is a pilot project in eastern Africa (Uganda, Kenya, Tanzania, Malawi, Rwanda, Burundi, and eastern DRC) to ascertain the usefulness of the AfricaArray network and data and various GEM products and tools such as the ISC-GEM catalogue, ground motion prediction equations and the OpenQuake package in improving seismic hazard assessment. The second phase is an assessment of risk in Addis Ababa. Should these projects prove successful, we hope to expand the effort to other parts of the African continent.

1.3 Geology and seismotectonic settings

Sub-Saharan Africa is largely a stable intra-plate region characterized by a relatively low level of seismic activity, with earthquakes randomly distributed in space and time. The only parts that do not display the characteristics of an intra-plate region are the East African Rift System (EARS) and the Cameroon Volcanic Line, where earthquakes are associated with active fault zones and volcanic activity, respectively.

The African continent is a palimpsest recording a lengthy tectonic history, and the EARS is superimposed on structures formed during earlier tectonic episodes. On a broad scale, much of it can be explained by plate tectonics and the Wilson cycle, for example to amalgamation and dispersal of Gondwana. However, there are other phenomena, such as the rise of the

African superswell, that are not well understood. The East African Rift System (EARS) stretches quasi-continuously from the Afar depression in northern Ethiopia to the Southwest Indian Ocean Ridge (SWIR) at the junction with the Antarctic plate. It is the southern branch of three rifts that radiate from a triple junction. The northwestern rift lies along the axis of the Red Sea, while the northeastern rift bisects the Gulf of Aden reaching an oceanic triple junction where meets the Indian Ocean Ridge. The EARS includes the world's youngest continental flood basalt province (Ethiopia) and is superimposed on a broad region of high topographic elevation (the 1000 m high eastern and southern African plateaus). This high elevation region and its offshore extension in the southeastern Atlantic define the "African Superswell" (Nyblade and Robinson, 1994), which lies on average 500 m higher than the global topographic mean. The analysis of long-wavelength gravity and topographic relief over Africa shows that more than half of this anomalous topography is dynamically supported (Lithgow-Berteloni and Silveri, 1998; Gurnis et al., 2000) by convective mantle upwelling associated with a large, slow shear wave seismic velocity mantle anomaly, the African superplume (Ritsema et al., 1998). The initiation of Cenozoic rifting is estimated to start in the mid-Tertiary with the onset of volcanism in the Turkana Rift (Furman et al., 2006) followed by uplift and flood basalts in Ethiopia (Pik et al., 2003). The process was followed by extension in the Main Ethiopian Rift and the western and eastern (Kenya) branches (Roberts et al., 2012), and further south in the Malawi Rift (Lyons et al., 2011).

1.4 Earthquake risk in the East African Rift System

Damaging earthquakes with M>6 occur almost annually in the East African Rift. Five M>7 earthquakes have occurred in eastern Africa since 1900, the largest known event being the 13 December 1910 Ms 7.4 Rukwa (Tanzania) event that badly cracked all European-style houses in towns on the eastern shore of Lake Tanganyika (Midzi et al., 2014; Ambraseys, 1991b; Ambraseys and Adams, 1991). A Ms 6.9 earthquake that occurred on 6 January 1928 in the Subakia Valley (part of the Kenya Rift, some 200 km northwest of Nairobi) produced a 38 km long surface rupture with a maximum throw of 2.4 m and destroyed, or damaged beyond repair, all European-style houses within 15 km of the rupture, fortunately without causing casualties (Ambraseys, 1991a).

During the last decade there have been several other events that have caused loss of life (Durrheim, in press). On 5 December 2005 an Mw 6.8 event caused several deaths and damaged school buildings and hundreds of dwellings in the Democratic Republic of Congo and western Tanzania. The 22 February 2006 Mozambican Mw 7 earthquake was one of the largest ever recorded in southern Africa, producing a surface rupture with a displacement of more than 1 m. Shaking was felt as far away as Zimbabwe and South Africa. Four people were killed, 27 injured, and at least 160 buildings damaged. On 3 February 2008 an Mw 5.9 earthquake struck the Lake Kivu region of the DRC and neighboring Rwanda. The event was located approximately 20 km north of Bukavu, DRC. The main shock was followed by

a second earthquake 3½ hours later. Numerous buildings collapsed or suffered significant structural damage, trapping many people under rubble. At least 40 people died and more than 400 were injured.

While these events caused relatively small losses, the populations has increased enormously over the last century and urbanized. Building methods have changed from wattle and daub or timber with grass roofs, which have a large inherent resistance to earthquake shaking, to European-style unreinforced masonry constructions, which are far more vulnerable to shaking. The occurrence of similar events close to a town would likely cause serious human and economic losses today. Africans cannot be complacent. A damaging earthquake could occur anywhere in Africa, although the frequency is greatest in tectonically active regions such as North Africa and the East African Rift System.

2. An Harmonised Earthquake Catalogue for SSA

2.1 Compilation of a SSA-GEM Catalogue

Starting point for PSHA analysis is the definition of the seismicity characteristics for the study area. This can be done in multiple ways, but the basic - and probably the most common - approach is in the use of an earthquake catalogue. Such catalogue is an as much as possible complete record of all earthquake events indirectly reported (the *historical* and *macroseismic* component) or directly recorded (the *instrumental* component) on a specific area and over a certain time span.

For each element (event) of the catalogue it is essential to report at least:

- **Location** - epicentral or hypocentral, depending on the availability (and the reliability) of depth solutions;
- **Time** - minimum requirement is the year for historical large events, but accuracy at the level of second (or fraction of a second) is advisable for recent instrumental events;
- **Intensity measure (IM)** - different parameters and scales are available; type of IM should always be reported with the catalogue (unfortunately not always the case).

Optional, but rather useful, is the reporting of the related uncertainties, while supplementary information is the source mechanism and various processing metadata (agency code, bibliographic references, etc.).

If several catalogues are available for a given study area, information can be quite heterogeneous and some objective criteria for selection, merging and homogenisation are needed. This is usually the case when neighbouring agencies are reporting same events but with different magnitude types. Same issue is affecting source solutions, for instance when different earthquake phases, processing algorithm or base model assumptions (e.g. earth velocity structure) are used.

GEM has recently developed a set of open-source tools that helps scientists going though the catalogue harmonisation process. In this study we make use of these tools (aka *GEM*

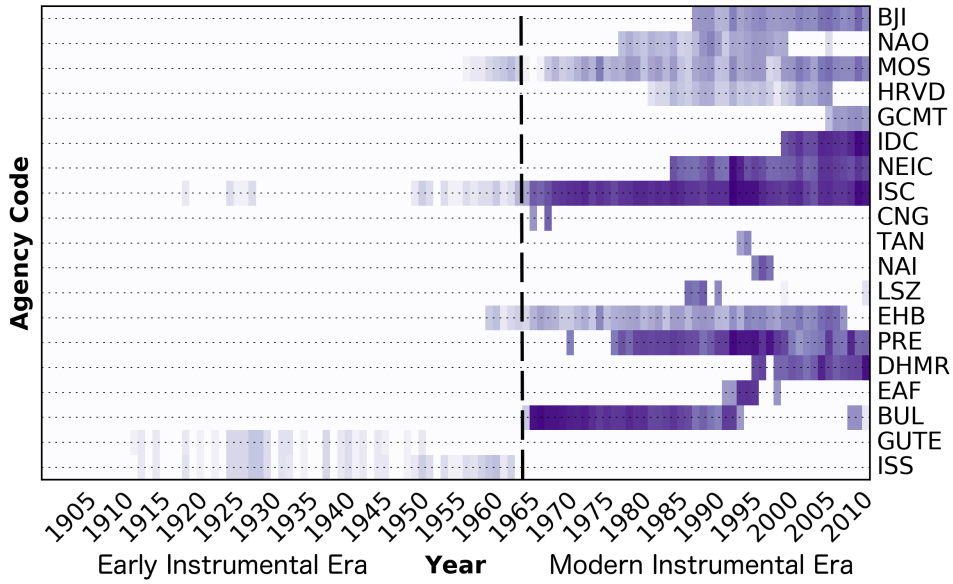

Figure 2.1 – *Time histogram showing the density (relative number) of events reported for some selected agencies of the ISC-REV bullettin which are potentially relevant for SSA hazard model.*

Catalogue Toolkit) to produce a state-of-art earthquake catalogue for Sub-Saharan Africa with homogenous magnitude representation (Mw). Such catalogue (hereinafter *SSA-GEM*) was created by augmenting available global catalogues (e.g. ISC-Reviewed, ISC-GEM, GCMT) with information from local agencies and regional projects, particularly from the AfricaArray framework. In the following we describe in detail the necessary steps, main assumptions and choices we faced to set up the SSA-GEM catalogue.

2.2 Available Global and Local Information

2.2.1 *ISC Reviewed Bulletin*

The lastest available snapshot of the manually reviewed bulletin from the International Seismological Centre (ISC) was used as one of the primary source of information for earthquake solution. The ISC bulletin covers a period ranging from the beginning of the 20^{th} century to present days. In our geographic area selection ($-40°$ to $20°N$, $10°$ to $60°W$) it spans the period 1904-2013, for a total of 26322 events from 89 international and national (local) agencies. Magnitude scale representation is however not homogenous and varies between agencies and considered time period. See Figure 2.1 for a comparison of the activity period of some of the agencies reported by ISC that are relevant for the study region.

2.2.2 *ISC-GEM Catalogue*

The ISC-GEM global instrumental earthquake catalogue (reference) is a refined version of the ISC bulletin, which improves the accuracy on magnitude and location solutions for large global events (Mw $>$ 5.5) in the period 1900-2012. Events reported the ISC-GEM

catalogue are considered as reference events, which have priority on other estimates from global bulletins. Intensity is homogeneously represented by using moment magnitude (Mw) from globally calibrated magnitude conversion relations. ISC-GEM catalogue is presently in its version 3, which is the one used in this study. 285 events (out of 24375) are available for the selected study region.

2.2.3 *Harward/GCMT Bullettin*

The Global Centroid Moment Tensor catalogue (CGCMT, Ekström et al., 2012) is a collection of moment tensor solutions for earthquakes with Mw > 5. The catalogue covers the period 1972 to present days, with a total of more than 25000 global events, 614 of which are of interest for this study. The GCMT record is fully integrated into ISC bulletin, but due to delays introduced by the review process, most recent events (presently after 2013) can only be obtained by direct parsing the catalogue. Note that within ISC bulletin, the Global Centroid Moment Tensor catalogue is indicated with two separated agency labels, *HRVD* and *GCMT*, indicating the migration of the project from Harvard (*Harward CMT Project*) to the Lamont-Doherty Earth Observatory (*LDEO*) of the Columbia University in 2006. Moment tensor solutions from the GCMT are considered as reference for the calibration of magnitude conversion relations used in this study (see section 2.4).

2.2.4 *GEM Historical Earthquake Archive*

The GEM Historical Earthquake Catalogue (GEH) is a global collection of reviewed historical records consisting of 825 events (M > 7) covering the period 1000-1903 (pre instrumental period). Unfortunately, only eight earthquakes from the GEH catalogue are relevant for the study region. This is likely due to the lack of historical records in sun-Saharan and central Africa. This poses the problem of completeness of the regional earthquake record for large magnitudes, which consequently affects and potentially bias the calibration of annual occurrence rates for these events.

2.2.5 *AfricaArray regional earthquake catalogues*

Aside from using information from global agencies, we extended the Earthquake record by integration of three local catalogues developed within the frame of the AfricaArray project. These catalogues are the result of regional earthquake monitoring performed with temporary and permanent seismic network installations.

Available AfricaArray catalogues are:

- The **Tanzanian Broadband Seismic Experiment** (labeled *TZB*), with 2218 events covering the period 1994-1995 and magnitude between 1.43 and 4.42;
- The **Ethiopian Plateau Catalogue** (labeled *ETP*), with 253 events covering the period 2001-2002 and magnitude between 1.75 ad 4.05;
- The **AfricaArray Eastern Africa Seismic experiment** (*AAE*), with 1023 events in the period 2009-2011 and magnitude range 1.28-4.04.

Although these catalogues extend the record to very low magnitude, the main implication for the present hazard study was in the use of these events for the local definition of seismicity distribution patterns and the subsequent improved design of a new area source model for Sub-Saharan Africa.

2.3 Earthquake Location Solutions

As a general rule, preference for earthquake location solution should be given to local agencies, while solutions from global agencies and teleseismic events should be alternatively used in those cases where local agencies are not available on the territory (e.g. not yet established) or when too large solution uncertainty exists, e.g. due to insufficient station coverage.

For the case of Sub-Saharan Africa, although solutions from several local agencies are made available through ISC bullettin, there is a general lack information regarding network operation (particularly before 1980) and metadata, including quality of the solutions, which makes the use of their locations often questionable. For these reasons, we decided to mostly rely on solutions from global agencies, while restricting the use of local agencies only to those cases where no other information was available.

By mapping the activity period of the different seismological agencies over time, we identify five main time intervals with a different scheme of agency prioritisation (see summary table 2.1). In the first period (pre-instrumental or historical era) only historical events from the GEM Earthquake Historical Catalogue (GEH) are considered. The second and third periods (early instrumental era) rely on global bulletins from international agencies, while the fourth and fifth periods (modern instrumental era) can also benefit from the contribution of local agencies, particularly for localisation of small-magnitude regional events.

Period	Agency selection
1000 - 1900	GEH
1901 - 1959	ISC-GEM, ISC, ISS, GUTE, GEH
1960 - 1964	ISC-GEM, EHB, ISC, ISS, GEH
1965 - 1980	ISC-GEM, EHB, ISC, NEIC, IDC, GCMT, HRVD, GCMT-NDK, BUL, PRE, LSZ, TAN, CNG, GEH
1981 - 2015	ISC-GEM, EHB, ISC, NEIC, IDC, GCMT, HRVD, GCMT-NDK, AAE, ETP, TZB, PRE, LSZ, NAI, TAN, CNG, EAF, GEH

Table 2.1 – *Prioritisation of agencies for preferred location solution. Selection is done differently for separated time periods, accounting for network operation and reliability of the estimate.*

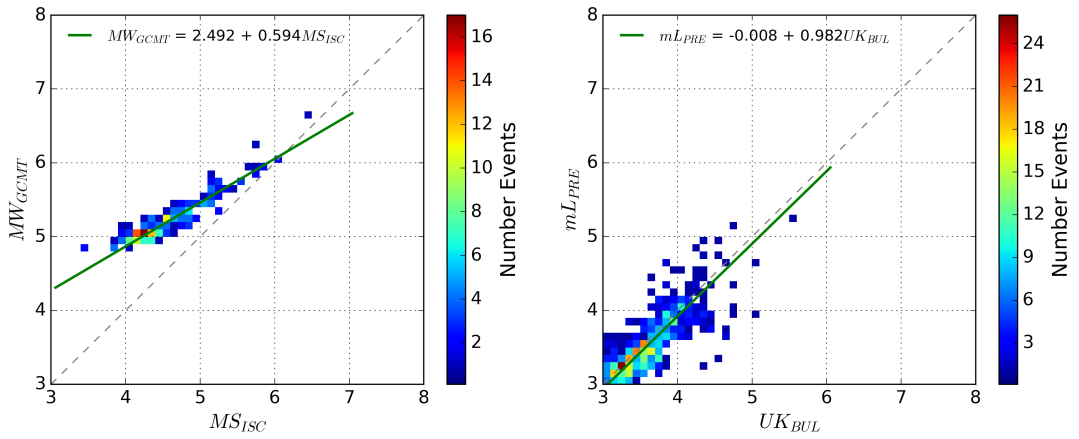

Figure 2.2 – *Example of regression model comparing ISC Ms events to reference GCMT Mw (on the left) and an unknown magnitude type from agency BUL to PRE Ml (on the right).*

2.4 Magnitude Conversion Rules

Seismicity analysis requires the seismic record to be homogeneously represented in term of intensity measure (*IM*). This is essential to avoid inconsistencies due to the different processing schemes used for different magnitude scales and the manifestation of saturation effects. These factors can heavily bias the subsequent calibration of magnitude occurrence relations.

Among different IM scales that can possibly be used as reference IM measure, the most natural choice is definitely the moment magnitude (Mw). This is due to its direct connection to earthquake size and energy and the absence of a saturation level. However, events with a native (directly obtained from data) estimate of Mw are limited, and very often a conversion from other scales is necessary. Although a conversion procedure allows producing an homogenous representation of the earthquake record, the downside stays in the introduction of some uncertainty related to conversion process, which relies on statistical regression models calibrated on available data from local or global datasets (reference paper Graeme).

For the definition of *ad-hoc* magnitude conversion rules, we used in this study the functionalities offered by the GEM catalogue toolkit (reference), which allow the exploration and statistical analysis of those earthquake events with multiple magnitude representations. For best results, calibration of regional conversion rules from local data is generally advisable. However, its feasibility strongly dependents on data availability. If a sufficient number of local events is not available for a given IM pair, two alternative approaches are then possible. First, a two-step conversion with an individual *dummy* magnitude of larger availability can be used. Alternatively, globally calibrated conversion rules can be applied. The first approach has to be considered carefully, as it results in the accumulation of uncertainty from each conversion step. The second approach might provide better estimates, given that well-represented worldwide agencies are analysed.

Agency	Type	Mw Conversion Rule	Range	Note
GCMT	Mw	None	–	–
ISC-GEM	Mw	None	–	–
NEIC	Mw	None	–	–
ISC	Ms	0.616*Ms+2.369	Ms<6	Weatherill et al., 2016
		0.994*Ms+0.1	Ms>6	
ISC	mb	1.084*mb-0.142	mb<6.5	Weatherill et al., 2016
NEIC	Ms	0.723*Ms+1.798	Ms<6.5	Weatherill et al., 2016
		1.005*Ms-0.026	Ms>6.5	
NEIC	mb	1.159*mb-0.659	mb<6.5	Weatherill et al., 2016
PRE	Ml	Ml	Ml<6	Assuming linear scaling to Mw and arbitrary large uncertainty (0.3 units)
BUL	Mblg	Ml	Ml<6	Assuming equivalence to PRE-Ml
TZB	Ml	$1.02+0.47*Ml+0.05*Ml^2$	Ml<5	Edwards et al., 2010
ETP	Ml	$1.02+0.47*Ml+0.05*Ml^2$	Ml<5	Edwards et al., 2010
AAE	Ml	$1.02+0.47*Ml+0.05*Ml^2$	Ml<5	Edwards et al., 2010
PAS	Ms	0.616*(Ms-0.2)+2.369	Ms<6	
		0.994*(Ms-0.2)+0.1	Ms>6	Using ISC-Ms conversion scaled by factor 0.2 (according to Engdahl and Villaseñor, 2002 - *Centennial Catalogue*)

Table 2.2 – *List of magnitude agencies and Mw conversion rules. Agencies are sorted according to decreasing priority for the catalogue harmonisation.*

For SSA region, we experienced a substantial lack of data for a proper calibration of local Mw conversion rules, and in most cases we had to rely on globally calibrated relations (e.g. ISC and NEIC, see table 2.2 for a complete list). However, few example cases deserve some discussion. ISC catalogue doesn't report any magnitude type for the local agency BUL (Goetz Observatory, Zimbabwe), but after direct comparison with other local agencies, we discover a strong correlation, although for a limited range of rather small magnitudes, with agency PRE (Council for Geoscience, South Africa), which is reported as a Ml estimate (see Figure 2.2). Since Ml scales roughly linearly with Mw for magnitudes lower than 6, we therefore decided to include BUL events in the homogenised catalogue, due to their large availability (about 10719 events). Nonetheless, to account for the large uncertainty of the assumed conversion, we assigned an arbitrarily (large) uncertainty of 0.3. We subsequently obtained confirmation that BUL magnitude are referred to as Mblg and have to be considered reliable

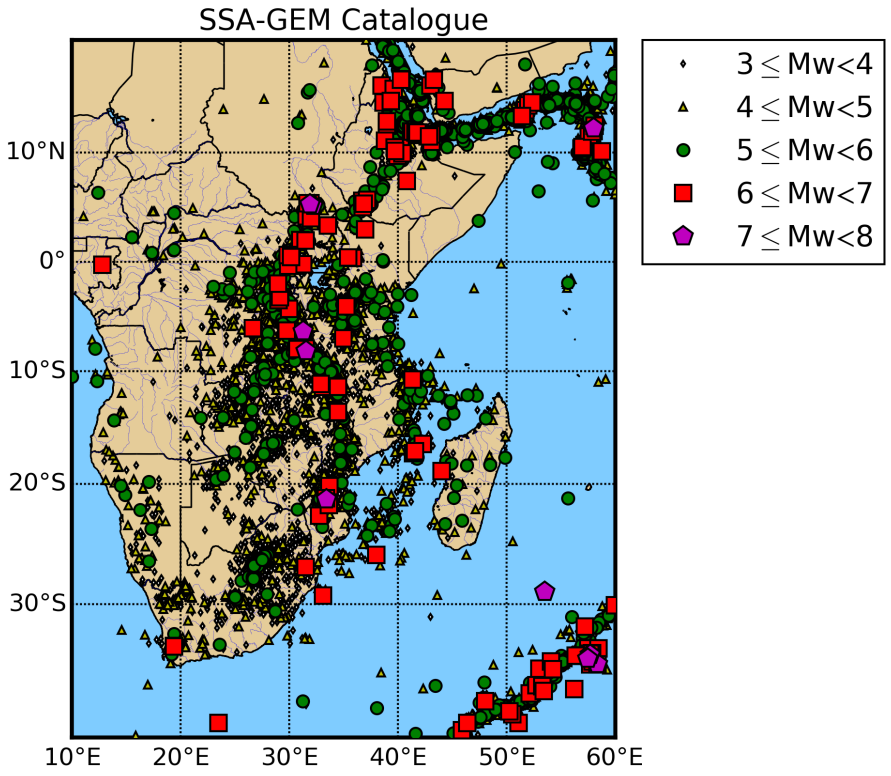

Figure 2.3 – *Distribution of earthquakes events of the homogenised SSA-GEM catalogue.*

up to around 1984.

Events from local *AfricaArray* networks TZB, ETP and AAE have also been originally reported in Ml scale. In this case, however, we assumed a more accurate magnitude estimation then the previous cases. This led us opting for a more sophisticated conversion rule from a recent study (Edwards et al., 2010) and with a lower uncertainty (0.15).

2.5 Merging Catalogues and Duplicate findings

When merging different earthquake catalogues, one issue is the identification of duplicate events. To face this problem, we use a procedure algorithmically similar to the event declustering (see section 2.6), where events falling within a window of prescribed spatial and temporal width are assumed representing the same earthquake. After some testing, we obtained good results with a window of 0.5° and 120*s*. These values appear sufficient to capture relative uncertainty in earthquake solution (traveltime and epicenter estimates) between agencies, which is particularly relevant for teleseismic events. The use of larger values is however not recommended, as this could erroneously affects the catalogue by capturing aftershocks sequences. After catalogue merging, previously defined priority rules for magnitude and location agency selection are applied and the final catalogue released (see Figure 2.3).

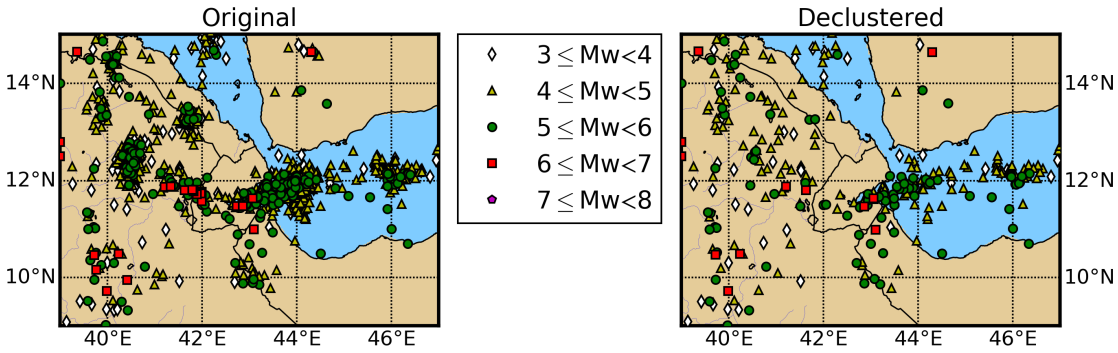

Figure 2.4 – *Comparing SSA-GEM catalogue before and after declustering of dependent events. It is show in this example the result for the Afar region, north Ethiopia. Five main aftershock clusters are identified and removed.*

2.6 Catalogue Declustering

The poissonian assumption widely used in probabilistic seismic hazard analysis (*PSHA*) to express earthquake occurrence rates in term of probability requires temporal indepence of the observed events. Unfortunately, earthquake catalogues are usually affected by the presence of groups of related events (*clusters*), such as fore-/after-shocks and seismic swarms. In order to estimate poissonian rates of seismicity, those dependent events have to be removed by filtering the catalogue prior to the calibration of any occurrence relationship.

Such procedure is called *catalogue declustering* and several algorithms have been proposed in literature to face this issue. Among others, one of the most popular is from Gardner and Knopoff (1974), due to its conceptual and computational simplicity. The algorithm isolates and removes dependent events from a sorted catalogue by virtue of a fixed time-distance window centered on each assumed earthquake main shock and proportional to its magnitude. Although several window variants exist (see Uhrhammer, 1986 or Van Stiphout et al., 2012), we use the original magnitude-scaling relation of Gardner and Knopoff (1974).

Declustered catalogue consists of 7259 events out of the original 29803 in the magnitude range $3 \leq Mw \leq 7.53$ (see e.g. Figure 2.4).

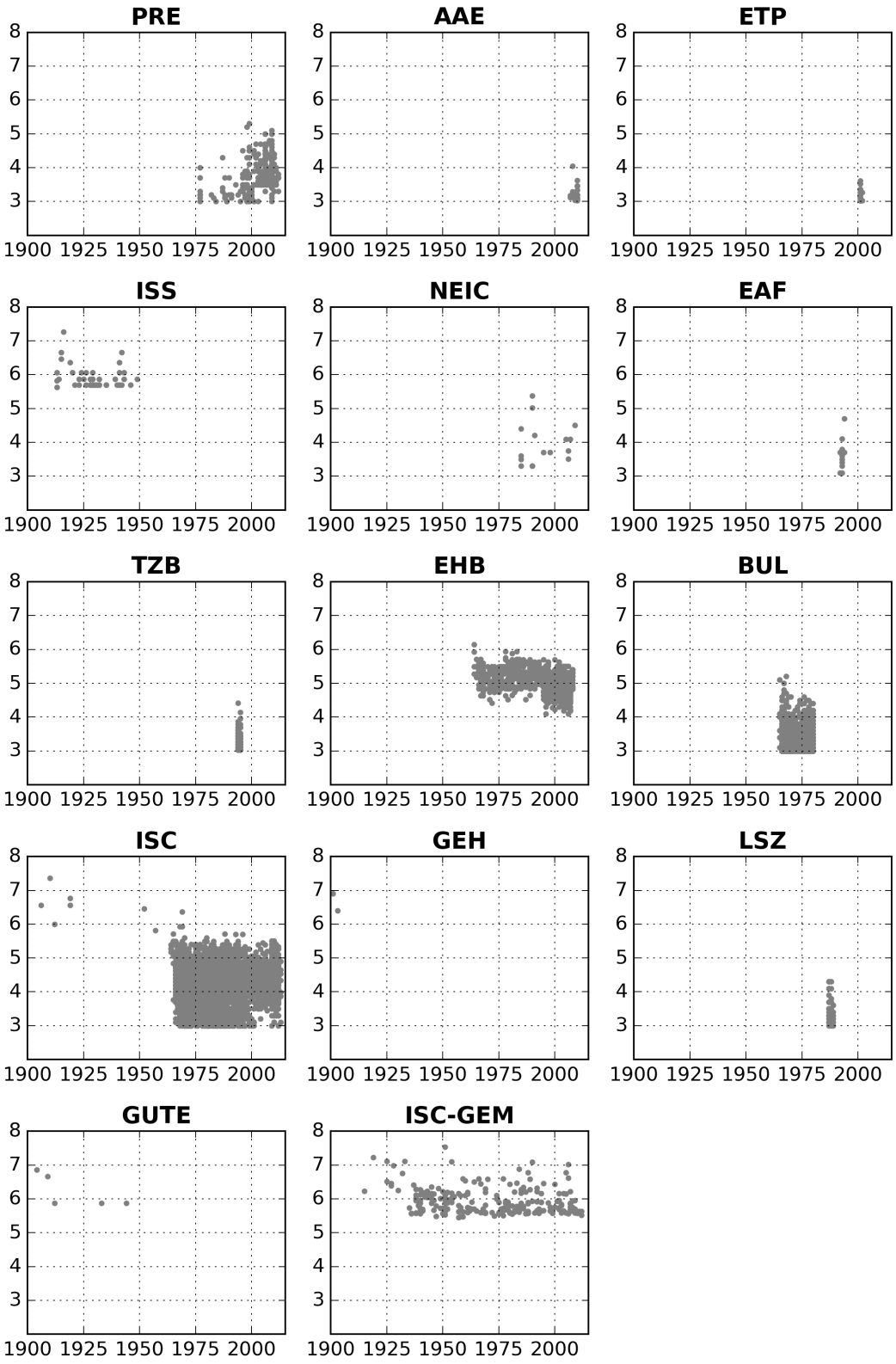

Figure 2.5 – *Relative contribution to the catalogue of the different agencies used for location solution. In each plot, time (in years) is on horizontal axis, while magnitude (Mw) is on vertical. Magnitude larger than 3 are presented.*

3. Area Source Model for Distributed Seismicity

3.1 Source Zonation

The proposed seismic hazard model for Sub-Saharan Africa is based on distributed seismicity, and requires the discretisation of the study area in source zones of supposedly uniform temporal and spatial earthquake occurrence. Such approach is commonly used when observed seismicity cannot be reliably linked to any known (or guessed) geologic structure, which is often the case of low seismicity regions. Main advantage of using area source zones (ASZ) stays in the straightforward implementation, although selection criteria might be highly subjective and often debatable between experts.

For the development of area source model we followed a mixed approach, which accounts for both observed seismicity (see figure 2.3) and the geological/tectonic characteristics of the study region. Such approach closely descends from the methodology advocated by (Vilanova et al., 2014), which consists in the definition of a set of objective criteria for ASZ boundary delineation. Seismicity constraints have been obtained from the analysis (completeness, occurrence rates) of the *ad-hoc* developed SSA Earthquake catalogue and it will be discussed in more detail in the next section. Aside, tectonic information was derived mostly from scientific literature and by integration of available datasets, such as the fault database of MacGregor (2015) and the plate boundary model proposed by (Saria et al., 2014). These last are summarised in figure 3.1.

The area source model (currently in its Version 5) consists of a total of 19 zones distributed over 6 main tectonic groups, which we assume of homogenous rheological and mechanical behaviour with respect to the underlying crustal geology. The definition of these groups is essential for the regional calibration of b-values, as it will be better described in the next sections. In the following, the main characteristics of each group are described in detail.

Group ID	Source ID	Name - Decription
1	02-00	South Read Sea
	03-00	Aden Gulf
2	01-00	Afar Depression - Eritrea
	04-00	Main Ethiopian Rift
	22-00	North Kenya - Lake Turkana
3	05-00	South Sudan
	07-00/01	Lake Victoria
	14-00	South Kenya
	20-00	Rowuma Basin
4	06-00	Western Rift - Lake Edward, Albert and Kivu
	08-00	Western Rift - Tanganika
	09-00	Malawi - Nyasa Rift
	18-00	South Mozambique
5	10-00/01	Walikale and Masisi
	11-00/01	Luama Rift
	12-00/01	Mweru - Katanga - Upemba
	13-00/01	Kariba - Okavango
6	15-00	Eastern Rift
	16-00	Davie Ridge
	17-00	Mozambique Channel

Table 3.1 – *List of area sources implemented in the current SSA source model. Last two digits of source ID indicates whether a zone have been implemented as a simple area (-00) or it includes an additional overlapping layer (-00/01).*

3.2 Group 1 and 2: Horn of Africa

The Afar Rift triple junction is a key point in the Arabia, Nubian and Somalia plate tectonics, because it represents the point of accommodation of three concurring extensional regimes, which are the Red Sea and Gulf of Aden spreading ridges to the North and the Ethiopian rift system to the South. The whole area is interested by a significant seismic activity and several large earthquakes have been observed in historical and modern times. For example, in 1969, a sequence of intermediate-size earthquake in Central Afar destroyed the city of Serdo, killing and injuring a substantial part of the population. During the 1989 Dobi graben (Central Afar) earthquake, several bridges on the highway connecting the port of Assabof Assab to Addis Ababa were destroyed (Kebede and Kulhanek, 1991). Surface geology and focal mechanism of earthquakes show that the whole region is dominated by normal faulting (Shudofsky, 1985; Kebede and Kulhanek, 1991), with a minor although not negligible strike slip component.

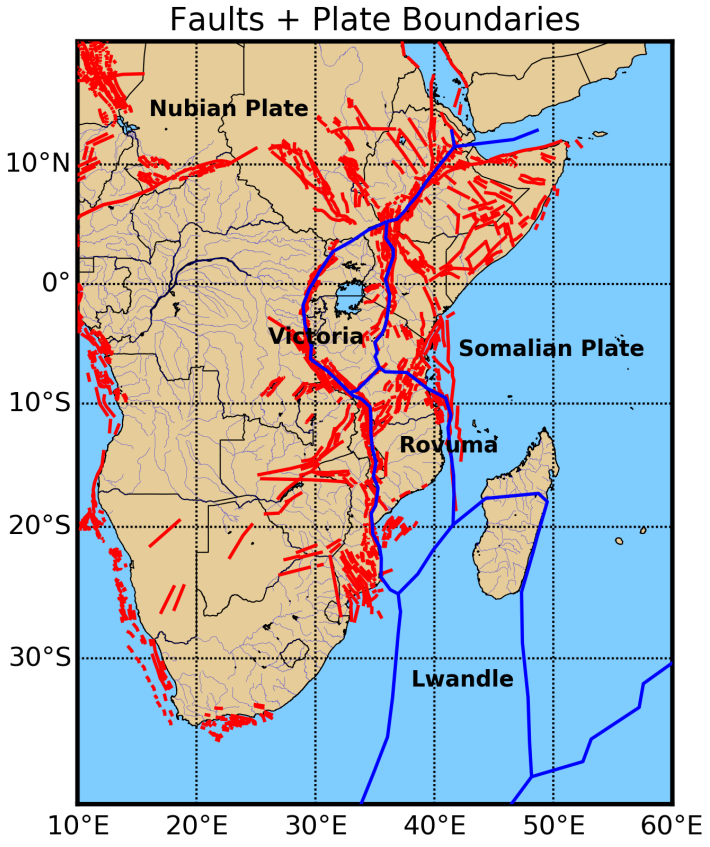

Figure 3.1 – *Main tectonic structures used as selection criteria for area source zonation: in red, faults from the database of MacGregor (2015); in blue, the plate boundary model of Saria et al. (2014).*

We formally separated the Red Sea and Gulf of Aden source zones (group 1) from the inland zones of the triple junction's southern branch (Afar, Ethiopian plateau and Ethiopian rift valley; group 2), which did not evolved (yet) in oceanic spread. The rationale behind this choice stays in the likely different seismic attenuation behaviour of the two neighbouring regions. However, this hypotesis has to be confirmed by analysis of local seismic recordings.

The Main Ethiopian Rift, in particular, is a single-extensional rift basin between Nubia and Somalia extending from the Afar triple junction (Wolfenden et al., 2004; Keir et al., 2009) to the Lake Turkana depression in northern Kenya. Few earthquakes focal mechanisms exist for the Ethiopian Rift and most of them show ESE-WNW orientation and normal fault (Casey et al., 2006).

3.3 Group 3: African Microplates

South of Lake Turkana, seismic and tectonic activity delineate two branches, the Eastern and Western Rifts, which bound a relatively unfaulted, scarcely seismic domain centered on a 2.5–3 Ga old assemblage of metamorphic and granitic terranes (Tanzanian craton). This domain has remained undisturbed tectonically since the Archean (e.g., Chesley et al., 1999), except for minor seismicity under Lake Victoria, and it was interpreted by Hartnady (2002) as the present-day Victoria microplate. Seismic, xenolith and gravity data show that the 150–200 km thick lithosphere of the Tanzanian craton is colder and stronger than surrounding

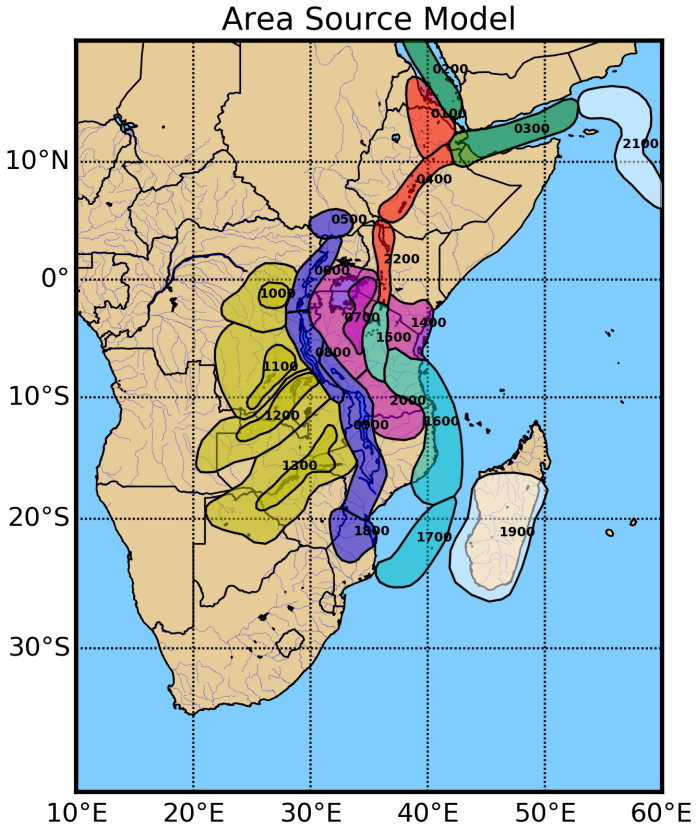

Figure 3.2 – *Source zonation model used in this study (see table 3.1 for details). Area sources belonging to the same group are represented with unique color. Additional source zones of Madagascar and the Indian See are also presented, but not used for hazard calculation.*

orogenic belts (Wendlandt and Morgan, 1982; Boyd and Gumey, 1986; Green et al., 1991; Ritsema et al., 1998; Weeraratne et al., 2003), which might lead to a less attenuating seismic propagation behaviour of the region. The low seismicity belt extends toward south of the Tanzanian craton and partially interests north Mozambique. This region, however, has been formally separated from the Victoria Microplate as the independent tectonic domain of the Rowuma microplate.

Although seismicity for these microplate regions is comparably very low with respect to neighbouring rifts zones, it still has to be represented into hazard model. This is done trough implementation of low-rates background area sources. Additionally to Victoria and Rowuma microplates, source group 3 partially extends to Nubian and Somalian plates to include the seismic clusters of South Sudan (to north-west) and Kenya (to the east). These regions have definitely higher seismic productivity, but they reasonably share a similar tectonic setup, which makes them suitable for the calibration of a common *b*-value.

3.4 Group 4: Western Rift System

This group contains four sources, which cover segments of the Western branch of the EAR, showing the highest rates of seismicity along the whole rift system. It includes the Albertine Rift (which contains the Albertine Graben, Semliki Basin and Ruwenzori Mountains), the Lake Kivu Basin including the Virunga volcanic area, Lake Tanganyika and Malawi. The present-

day fault kinematics as evidenced by the focal mechanism of events in the Albertine Rifts is normal faulting under NW-SE extension. Focal mechanisms in the Lake Kivu area display also a normal faulting with general trend N-S as opposed to the NE-SW of the Albertine-Ruwenzori segment. The Lake Tanganyika occupies the central part of the Western Branch. The stress inversion for North Tanganyika gives an ESE-WNW under Normal Faulting regime with a slight strike slip component. The southern part belongs to the TRM (Tanganyika-Rukwa-Malawi) rift segment, along which the kinematic model of Chorowicz (2005) infer dextral strike slip movements under NW-SE extension. The Rukwa Rift forms the central part of the TRM segment. In addition, the Ufipa Plateau between the Rukwa and South Tanganyika depression is affected by the 160 km-long Kanda active normal fault that might have generated the 1910 Ms 7.4 earthquake., which is the strongest ever recorded in the east Africa Rift (Vittori et al., 1997; Delvaux and Barth, 2010a).

Most of the seismicity of the EAR is concentrated in the magma-poor Western Rift, which initiated around 25 Ma simultaneously with the Eastern branch (Roberts et al., 2012). The Western branch is characterized by low-volume volcanic activity, large ($M > 6.5$) magnitude earthquakes, and hypocenters at depths up to 30–40 km (Yang and Chen, 2010; Craig and McKenzie, 2011). From Lake Albert to southern Rukwa, the width of the Western branch does not extend more than 40–70 km, with large volcanic centers coincident with the basin segmentation (Virunga, South-Kivu, and Rungwe). The Western Rift connects southward with the Malawi Rift via the reactivated Mesozoic Rukwa Rift (Delvaux et al., 2012). The Malawi Rift itself shares similarities with the Tanganyika basin, with long and well-defined normal faults (e.g., Livingstone escarpment) and limited volcanism. The 2009 Karonga earthquake swarm, with 4 $Mw > 5.5$ events (Biggs et al., 2010), however, showed that additional hanging wall normal faults participate in present-day extension. Recent coring in Lake Malawi indicates that modern rift initiation may be as young as early to middle Pliocene, considerably younger than most prior estimates (Lyons et al., 2011).

Craig and McKenzie (2011) found that seismicity (i.e. centroid depths) is confined in the uppermost 11 km. The seismicity observed within these areas shows very few events before 1960, probably because of the lack of seismic stations. The maximum magnitude observed corresponds to 7.3 (Mw); this was generated by the 1910 earthquake occurred in Rukwa. The accuracy of the focal depth is generally poor owing to the sparse station spacing. However, micro seismic studies indicate that earthquakes are generally between depths of 10 to 20 km in the Western Rift Valley (Zana, 1977; Zana and Hamaguchi, 1978).

3.5 Group 5: Continental Africa

Masisi is located at the northwest of Lake Kivu. A study of earthquake focal mechanisms by Tanaka and Zana (1980) showed that the direction of the fault traces in that area is SE-NW, and the average focal mechanism is normal faulting with the tension axis perpendicular to the strike of the fault traces. The last strong earthquake occurred in the Masisi area on 29

April 1995 (Mb 5.1) (T., 2007).

The most prominent seismotectonic features in this region are the Upemba and Moero or Mweru Rifts. The Upemba Rift is characterized by a NE-SW striking fault extending along its eastern side (Studt et al., 1908). The Upemba Rift may extend northward to the Kabalo area, which experienced an earthquake with magnitude Mw6.5 on 11 September 1992. In the city of Kabalo, the poorly constructed brick buildings experienced the most severe damage. The main shock claimed 11 lives and 109 people were seriously injured (4 died within a month of the main shock). More than 2000 families were left homeless. Detailed investigation has revealed that the main geological features in the Kabalo area trend in the NNE-SSW direction, similar to those found in the Upemba Rift (Zana et al., 2004).

The filling of Lake Kariba on the Zambezi River and subsequent fluctuations of water level have been accompanied by seismicity. Kariba Dam was built from 1955-1959, and is one of the world's largest dams. The wall of the Kariba Dam is 128m high, and the reservoir is 280 km long and has a storage capacity of 180 km^3. Seismic loading was not taken into account during the design of the dam, even though the reservoir is located in a tectonically-active branch of the East African Rift system and a Ms 6.0 earthquake had occurred in the region in 1910. No local measurements of seismicity were carried out prior to the impoundment, but many studies were carried out after 1959 (World Commission on Dams, 2000). Seismic activity increased as the dam filled, and peaked in 1963. The larger earthquakes (M>5) occurred in the vicinity of the dam wall. The largest event (Ml 6.1, which occurred in 1963) caused damage to the dam structure and some property in nearby settlements. No casualties were reported. Since 1963 there has been a general decline in seismic activity.

3.6 Group 6: Eastern Rift System

The Eastern Rift branch is characterized by a broad zone of shallow (5–15 km) and smaller magnitude seismicity, but voluminous volcanism (e.g., Dawson, 1992; Yang and Chen, 2010; Craig and McKenzie, 2011). The Eastern Rift includes the 25 Ma Turkana Rift, which reactivates part of an Eocene-Oligocene rift system (George et al., 1998; Pik et al., 2006). South of Lake Turkana, rifting and volcanism initiated at about 25 Ma (Furman et al., 2006; McDougall and Brown, 2009) with active eruptive centers along its length and moderate seismic activity. The seismically active southernmost part of the Eastern Rift, < 5 Myr old in the Natron basin, experienced in 2007 a discrete strain accommodation event rarely observed in a continental rift, with slow slip on a normal fault followed by a dike intrusion (Calais et al., 2008; Biggs et al., 2009).

South of the Natron basin, the Eastern branch of the EAR splits into the Pangani, Manyara, and Eyasi Rifts at an apparent triple junction (North Tanzanian Divergence, NTD) (Le Gall et al., 2004). The continuation of the Eastern branch south of the NTD appears more prominent along the Manyara Rift (Macheyeki et al., 2008), which may therefore form the eastern boundary of the Victoria plate. The aseismic plateau between the Manyara and Pangani

Rifts has been interpreted as a microplate (Masai block), separate from Victoria and Somalia (Dawson, 1992; Le Gall et al., 2008). Farther south, the Manyara and Pangani Rifts connect with the Usangu basin to the southwest and with the Kerimbas Rift to the east. The presence of 17–19 Ma phonolites intruding the basin sediments (Rasskazov et al., 2003) indicates that the Usangu basin likely initiated in the early stage of rift development. The Usangu basin shows moderate seismicity and connects to the south with the Malawi Rift, while the Kerimbas Rift is continuous offshore with the Davie Ridge, a narrow, NS trending, zone of seismicity with purely east-west extensional focal mechanisms (Mougenot et al., 1986; Grimison and Chen, 1988). The southward continuation of the Davie Ridge is unclear, but it may connect with the Quathlamba Seismic Axis, a linear cluster of seismicity between Madagascar and southern Mozambique (Hartnady, 1990; Hartnady et al., 1992).

South of the Malawi Rift, active deformation extends along the seismically active Urema graben and further south along the Chissenga seismic zone and the Urrongas protorift swell (Hartnady, 2006), where the Mw 7.0 Machaze, Mozambique, earthquake of 23 February 2006 occurred (Fenton and Bommer, 2006; Yang and Chen, 2010).

From the study of focal mechanism, Delvaux and Barth (2010b) deduced that an E-W extension occurs along the Davie Ridge. This ridge is considered to be the southward continuation of the Eastern Branch of the EARS.

The Western Branch of the EARS continue south of the Mbeya triple junction by the Malawi Rift and by more weakly expressed asymetric structures along the coastal region of Central Mozambique. The Mbeya lies at the triple junction between the Somalia, Victoria and Rovuma plates (Ebinger, 1989; Delvaux and Hanon, 1993). It contains the Rungwe volcanic province and links the NW trending South Rukwa and North Malawi rift basins with the NE trending Usangu basin. In February 2006, a Mw 7.0 earthquake occurred in the Coastal region of Central Mozambique and generated a surface fault rupture observed over 15 km, with a possible overall extension of 30 km with a vertical separation from 0.4 to 2.05 m and a component of left-lateral displacement of maximum 0.7 m (Fenton and Bommer, 2006).

South of the Manyara-Dodoma Rift un Central Tanzania, active extensional deformation associated in the Eastern Branch of the EARS seems to jump laterally to the coastal region and the Indian Ocean. The coastal region of Kenya and Tanzania display homogeneous extension in an ENE-WSW orientation and a pure Normal Faulting regime. Between Mozambique and Madagascar, the Mozambique Channel is known for its seismicity associated mainly to the Davie Ridge.

4. Calibration of Seismic Source Properties

4.1 Depth Solution Distribution

Source depth distribution was calibrated based on earthquake catalogue information. Unfortunately, not all reported events included an estimation of hypocentral depth. In few cases, moreover, such estimate was not reliable because of the large uncertainty (generally for large depths) or because being assigned a-priory (e.g. fixed solution depths of 5, 10, 15 and $33Km$, see figure 4.1). These events have been removed from the analysis. Nonetheless, a sufficient number of samples were available to perform a reasonable statistic (table 4.1).

ID	N^{tot}	5Km	15Km	25Km	35Km
1	182	37	80	51	14
2	50	15	21	8	6
3	26	5	11	4	6
4	163	28	58	53	24
5	77	22	24	17	14
6	69	12	30	16	11

Table 4.1 – *Number of events for which a depth solution is available. The events are geographically divided by source group and are clustered into four main depth categories of* $10Km$ *width.*

4.2 Source Mechanism

Geometry of a source can be described by focal mechanism parameters *strike*, *dip* and *rake*. While strike and dip uniquely describe fault orientation, rake is used to further specify the style of displacement (*normal*, *thrust*, *strike-slip* or *oblique*).

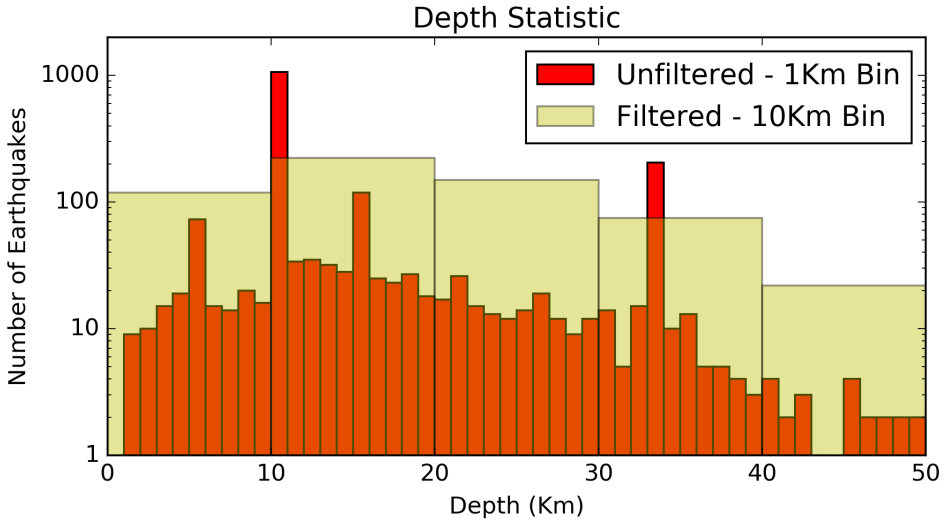

Figure 4.1 – *Distribution of the hypocentral depth solutions of those events falling into the main six source groups. From the plot it is evident the occurrence of peaks with unrealistically high occurrence. These are related to a-priory constraint on depth solution, and have been removed (filtered) from subsequent analysis.*

Source parameters can be derived as *fault-plane solution* from *moment tensor* inversion of earthquake recordings. If a sufficiently large number of events with tensor solutions is available for a specific area, a reliable statistic on source geometry and tectonic regime can be obtained. Alternatively, source style can be inferred from available information on local and regional stress regimes and the knowledge on existing geological structures. Given the scarce availability of recordings for the study region, not sufficient to perform statistical analysis, we proceeded using this last approach.

In a first step, we summarised the information available from scientific literature (see chapter 3). From that, main faulting styles of each source zone have been preliminarily delineated. For the whole study region, tectonic regime is generally extensional. A minor although not negligible transcurrent component is also present in some regions. We therefore modelled normal faults by imposing a standard dip angle of 60° and progressively adding strike-slip component (where necessary) by allowing oblique strike on fault plane. Since in most cases precise information on slip direction was not present, we allowed either left lateral (−45°) and right-lateral (−135°) components with equal probability.

Strike distribution has been calibrated by performing statistic analysis on fault structures available from the database of MacGregor (2015). To do this, fault lineaments were split into segments of fixed length ($1Km$), in order to weight differently segments of different length, but also to avoid issues related to arbitrary segmentation of main faults. Segment statistic was then used to constrain average strike orientation in each zone. In few cases, bimodal (and even more complex) distributions were found, which are due to a mixed tectonic regime.

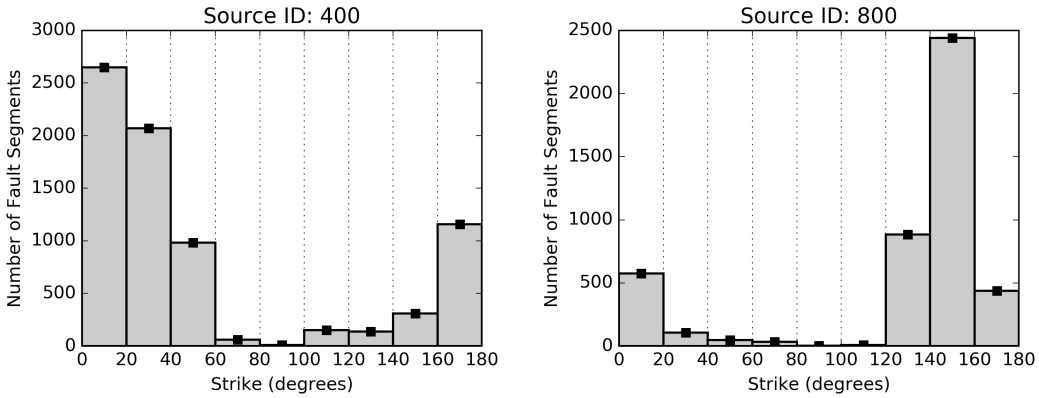

Figure 4.2 – *Statistical distribution of fault orientation for two example source zones (04.00 and 08.00). Input information is from the fault database of MacGregor (2015).*

As already mentioned, this was generally represented in our model by merging of normal component (dominating) and a strike slip component.

4.3 Seismicity Analysis

4.3.1 *Magnitude-Frequency distribution*

Seismicity of each area source zone is assumed to follow a double truncated Gutenberg-Richter magnitude occurrence relation (or magnitude-frequency distribution, MFD). In this model, lower truncation threshold is arbitrarily assigned to Mw4.5 for all zones. This is a standard choice in earthquake engineering, as it ideally represents the lower earthquake intensity capable of generating appreciable damage in the near field. Complementary, upper truncation level is defined as the magnitude of the larger earthquake assumed *possible* (or better *plausible*) for the area. A different maximum magnitude (Mmax) estimate is derived independently for each source group (see grouping in figure 3.2) as the largest *observed* event, plus an arbitrary - although quite conservative - increment of about 0.5 magnitude units. Nonetheless, to account for the large subjectivity of this choice, we allowed for a further relative variability of ±0.2 magnitude units in the source logic tree (see chapter 5).

Given these constraints, *b*-values have been initially calibrated for each source group, within which we assume similar mechanical behaviour of the underlying crust and therefore similar stress-drop and moment release scaling between small and large magnitudes. Subsequently, occurrence rates (*a*-values) have been calculated separately for each source zone (including aforementioned background and overlapping zones) by using the fixed *b*-values previously obtained for the groups. This strategy was necessary given the limited amount of data available for the study area, and particularly for those zones of quite limited extension.

It has to be mentioned that for the calibration of MFD parameters, other than just using standard and well-established approaches, such as the Aki's maximum likelihood (Aki, 1965)

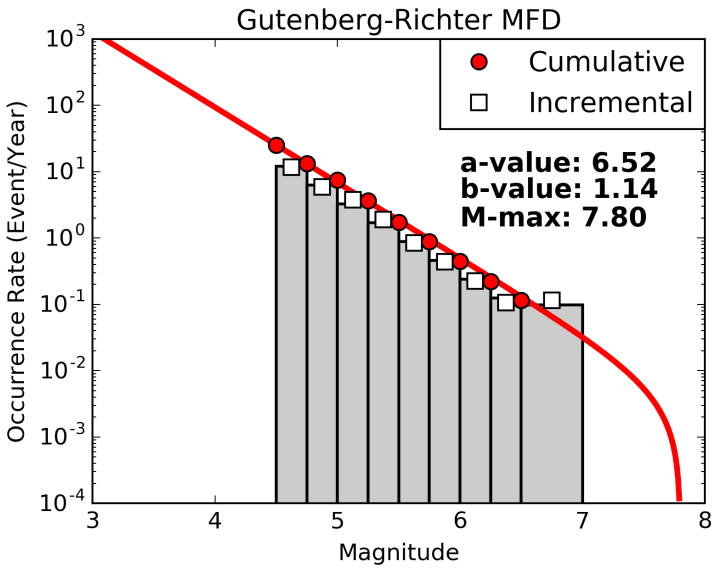

Figure 4.3 – *Example of Gutenberg-Richter magnitude occurrence relation calibrated on the whole declustered SSA dataset. Red solid line is the fitted relation, while symbols represents observer rates (cumulative and incremental) for discrete magnitude bins.*

and Weichert's methods (Weichert, 1980), we implemented a new strategy based on direct inversion observed earthquake occurrences. By using the assumed maximum magnitude, seismicity parameters (a- and b-values) can subsequently be obtained by minimizing the residuals between observed incremental occurrence rates in discrete magnitude bins and the theoretical expectation from a double truncated MFD model. The advantage of this strategy stays in the possibility of using bins of arbitrary width, not necessarily contiguous or continuous and to introduce arbitrary a-priori constraints (such as the use of a fixed *b*-value). Furthermore, this strategy allows rejection of those occurrence rates of uncertain calibration, as for the case of uncertain completeness of reported large magnitudes.

4.3.2 *Catalogue Completeness*

In the earliest stages of processing an instrumental seismic catalogue to derive inputs for seismic hazard analysis, it is also necessary to determine the magnitude completeness for different temporal periods. To outline the meaning of the term "magnitude completeness" and the requirements for its analysis as an input to PSHA, the terminology of Mignan and Woessner (2012) is adopted. This defines the magnitude of completeness as the "lowest magnitude at which 100 % of the events in a space-time volume are detected" (Rydelek and Sacks, 1989; Woessner and Wiemer, 2005). Incompleteness of an earthquake catalogue will produce bias when determining models of earthquake recurrence, which may have a significant impact on the estimation of hazard at a site. Identification of the completeness magnitude of an earthquake catalogue is therefore a clear requirement for the processing of

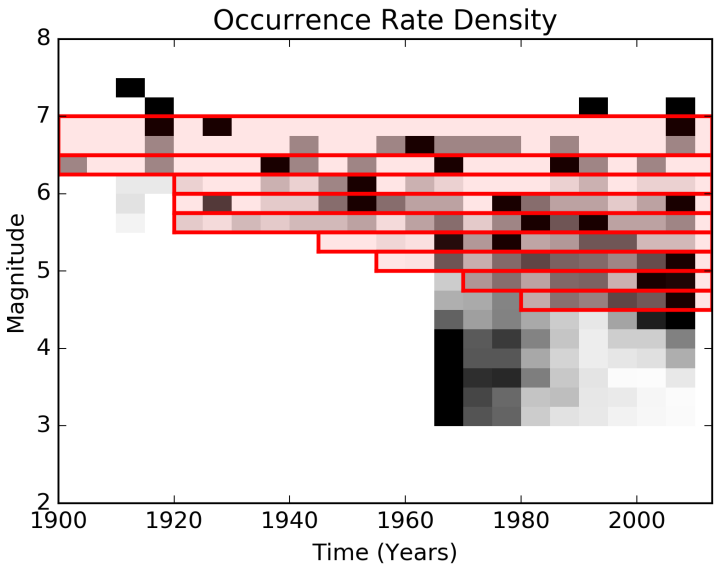

Figure 4.4 – *Example of manual identification of catalogue completeness on all events from the whole Sub-Saharan Africa region. On the background (with normalized grayscale) is the distribution of annual rates computed for discrete time windows. On top (in red) the completeness computed for separated magnitude bins (corresponding to the bins in figure 4.3).*

input data for seismic hazard analysis.

We identified appropriate time-magnitude completeness windows by comparing the results from two independent procedures. At first, we used the set functionalities made available in the GEM Hazard Modeller Toolkit (*HMTK*) and in particular the graphical implementation of the algorithm proposed by Stepp (1971). In cases of sparse data coverage, however, results from this automatic procedure might be relatively uncertain. This is unfortunately the case for Sub-Saharan Africa. A subsequent manual refinement is therefore necessary. We performed this second step by manually compare magnitude-frequency distribution obtained using progressively adjusted completeness tables. This process is iterated till a satisfactorily smooth and regular MFD is obtained.

The assessment of catalogue completeness was performed for the whole Sub-Saharan Africa region (e.g. figure 4.4) and for each identified area source zone separately.

4.3.3 *Earthquake Rate Redistribution*

In a previous step, seismicity parameters (a- and b-values) have been calibrated for each source zone. Subsequently, in order to avoid duplicate counts of events on overlapping zones (as the case for zones 12.00 and 12.01), redistribution of rates is necessary. Practically, background events have to be removed from the rates computed for the topmost overlapping layer, so that join calculation of the relative occurrence rates for the two zones will keep the total balance unmodified.

First, unit-area background rate is obtained by counting the occurrences in the background region not falling also into the overlapping layer. This can be done by simple subtraction of the total events observed in the two zones. The background rate is then removed from the occurrence of the overlapping zone after rescaling by local area extension.
Explicit formulation of the procedure would be:

$$N_{Back.} = (N_0 - N_1)\frac{A_0}{(A_0 - A_1)} \tag{4.1}$$

$$N_{Layer} = N_1 - (N_{Back.}\frac{A_1}{A_0}) \tag{4.2}$$

where N and A are respectively the number of events per year and the area extension for the different zones (0, 1, $Background$ and $Layer$).

For simplicity, we limited this procedure to just one single overlapping zone, but such strategy can nonetheless be extended to the use of several layers, each delimited by contouring the average density level of events over the area. This approach would be in a way intermediate between standard distributed and smoothed seismicity models.

5. Logic Tree Implementation

While aleatory (or *random*) component of the model uncertainty is generally taken into account by exploring the probability distribution of model parameters, the epistemic component, which is related to the available level of knowledge and/or the adopted initial assumptions and simplification, can be quantified by using a logic-tree strategy.

In a logic-tree approach, different interpretations of the model components are considered concurrently. Statistic analysis is performed *a-posteriori* on the weighted outcome of each model realisation (or logic-tree *branches*). OpenQuake allows the use of different branching *levels*, each of those representing a separate contribution to uncertainty. A multilevel strategy assures the full exploration of the model variability by computation of all possible permutations of those model parameters affected by epistemic uncertainty.

We applied this strategy to account for the difference between existing ground motion prediction models and for the variability of source parameters not directly constrained by available data.

5.1 Ground Motion Prediction Equations

Best strategy for the selection of most representative Ground Motion Prediction Equations (GMPE) is the direct comparison of empirical ground motion estimates with observed earthquake recordings in a sufficiently representative range of magnitudes and distances. The GEM Ground Motion Toolkit offers a set of simple functionalities to pursue this goal. Unfortunately, Sub-Saharan Africa is affected by a severe lack of data availability. The use of AfricaArray networks did not improve significantly the situations, due to too low magnitudes covered, lack of recordings in the near to intermediate distance range (<50km) and data accessibility restrictions (only recently solved by integration into IRIS database).

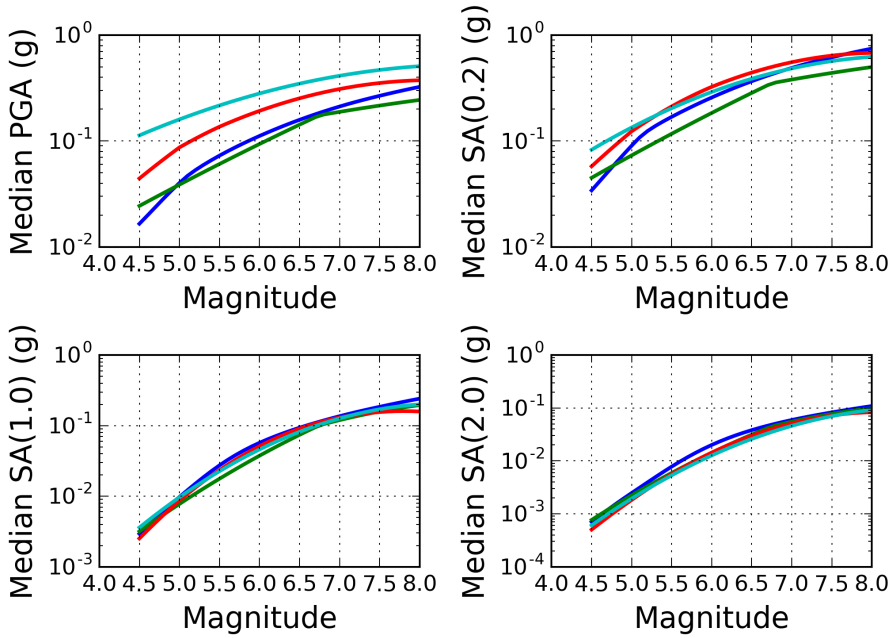

Figure 5.1 – *Variability in ground motion predicted by the four selected GMPEs versus magnitude and for different spectral ordinates. Color legend is described in the manuscript.*

For these reasons, we alternatively had to rely for GMPE selection on an simpler - but less accurate - selection criteria, based on direct evaluation and comparison of GMPE features, such as:

- The tectonic context of validity;
- Type and quality of data used for calibration;
- Suitability of the functional form.

In a first round, sixteen GMPEs from worldwide were selected as possible candidates, covering four different tectonic contexts:

- Active shallow crust (ASC);
- Stable continental crust (SCC);
- Cratonic areas (CRT);
- Volcanic areas (VLC).

However, ground motion predictions equations from CRT and VLC settings has been trimmed off nearly immediately, because of the questionable representativity on the investigated area and the lack of available data to perform ad-hoc seismicity analysis. This last issue is particularly critical in case of volcano-related seismicity, which is nonetheless a possibly significant contribution to seismic hazard at specific sites. Once more data will be made available, it is advisable that this component will be progressively integrated into the model.

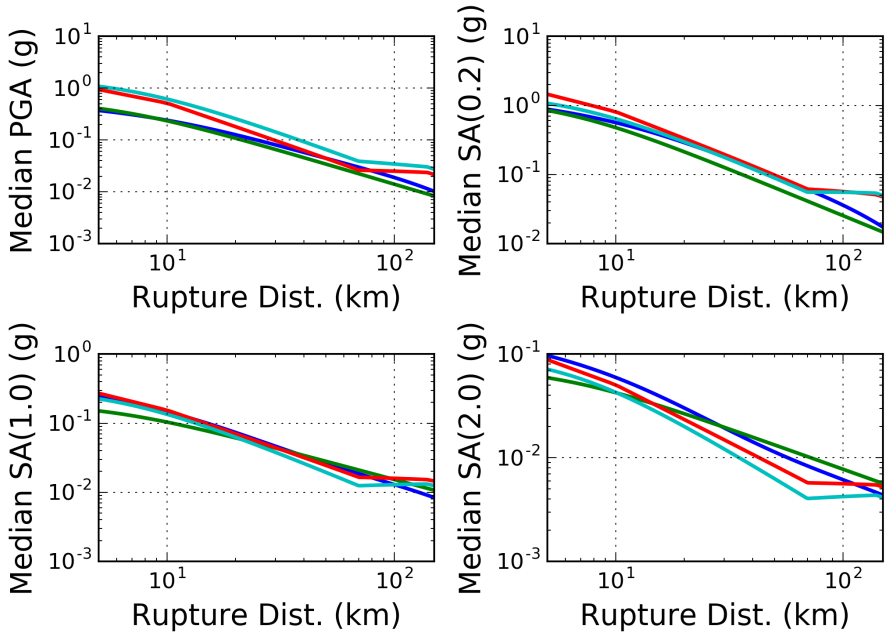

Figure 5.2 – *Variability in ground motion predicted by the four selected GMPEs versus J-B distance and for different spectral ordinates. Color legend is described in the manuscript.*

In a first attempt, GMPEs for ASC and SCC have then been assigned to different area source groups. While we used ASC GMPEs for areas involving plate boundary segmentation (groups 2, 4, 6), SCC GMPEs where used to model ground motion in all intra-plate areas (group 3 and 5). The rationale behind this choice is the evolution of the African rifting. Given the relative young age of the process, it might be expected extra-rift regions to be less exposed to asthenospheric upwelling, and therefore to preserve a mechanical behaviour and a seismicity footprint typical of stable continental areas.

However, after some sensitivity test calculation, we found that using a sharp separation between regions of different tectonic setting would have led to unjustifiable large differences in the computed ground motion across certain zone boundaries. In order to minimize such effect, while retaining the assumption of diversity in crustal attenuation and stress-drop, we proceeded with an alternative approach.

The current logic-tree model was restricted to the use of four GMPEs, respectively two for active shallow crust:

- Chiou and Youngs (2014) - CY
- Akkar et al. (2014) - AK

and two for stable continental conditions:

- Atkinson and Boore (2006) - AB
- Pezeshk and Tavakoli (2011) - PZ

We assigned all of the selected GMPEs to each source zone, but allowing the corresponding weights to vary in agreement with the likelihood of each specific tectonic type. Weight assignment was agreed on the base of direct judgement of local seismotectonic conditions from a pool of experts. The full list of weights is summarised in table 5.1. Zones sharing the same weighting scheme have then been clustered into four main groups (named A to D) to reduce the total number of end-branches into the logic tree implementation.

In figures 5.1, 5.2 and 5.3 it is presented a comparison of the selected GMPE for four best representative spectral periods (respectively at 0-PGA, 0.2, 1 and 2 seconds) and for a range of magnitude and distance values. Color code is: CY in blue; AK in green; AB in red; PZ in cyan.

Group ID	Source ID	CY	AK	AB	PZ
A	1, 2 3, 4, 17,	0.5	0.5	0	0
B	5, 6, 8, 9, 18, 22	0.375	0.375	0.125	0.125
C	15	0.25	0.25	0.25	0.25
D	7, 10, 11, 12, 13, 14, 16, 20	0.125	0.125	0.375	0.375

Table 5.1 – *Weighting scheme used for the GMPE logic tree. Source zones sharing the same weights are grouped into four main categories (A-D).*

5.2 Source Model Uncertainty

The source model logic tree has currently a master branch that includes the single area source zonation described in the previous chapter (Version 5). On top of that, additional branching levels have been implemented to describe the epistemic variability of the assumed maximum magnitude of each zone. Maximum magnitude is assumed to have a relative possible error of ±0.2, assigned empirically with a certain level of conservatism. The higher weight (0.5) is assigned to the original unmodified magnitude estimate, while edge values (±0.2) have a lower probability of 0.25 each.

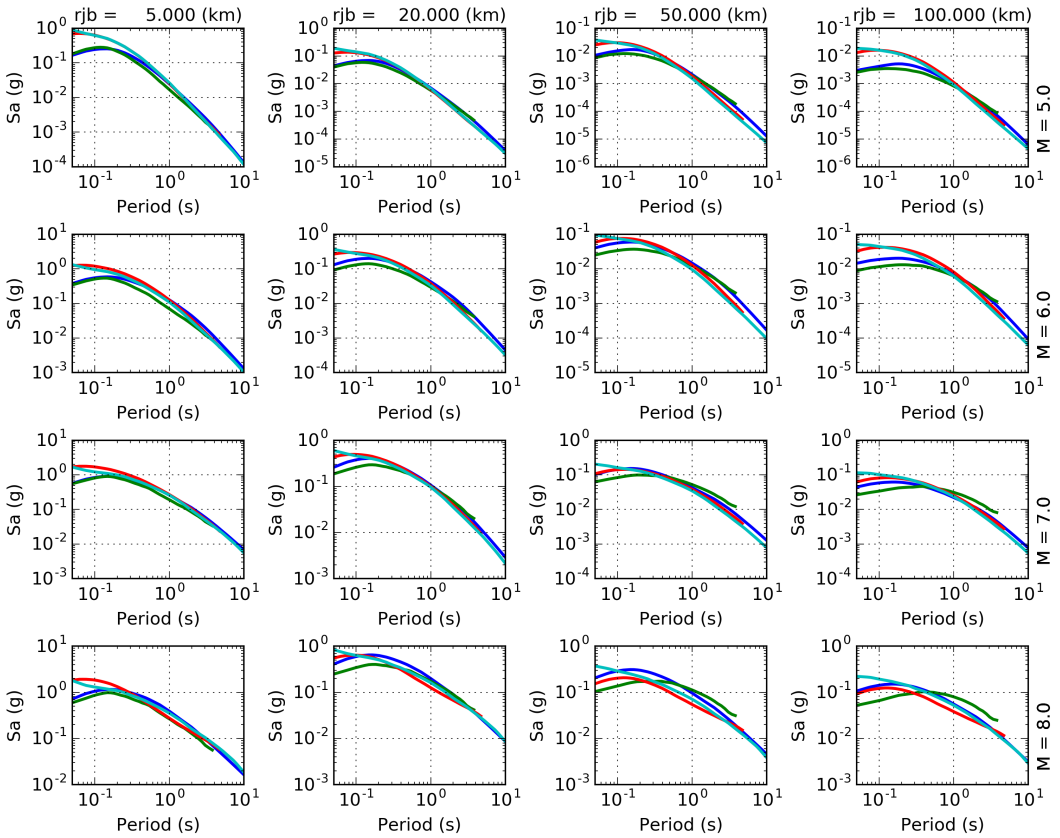

Figure 5.3 – *Summary comparison of full response spectra versus magnitude (along columns) and J-B distance (along rows) for the four selected GMPEs. Color legend is described in the manuscript.*

To avoid correlation of uncertainty among magnitude realisations from the different areas sources, an independent branching level was initially defined for each zone separately. Although this is a formally more correct approach than using a single branch implementation (which implied statistical correlation between model parameters, see figure 5.4 for clarification), it has the disadvantage to be computationally more demanding. However, after sensitivity comparison between the results from the two possible approaches, we opted for using the simple correlated model, being the maximum difference in ground motion of only 0.000025g, practically not relevant to justify the increased computational cost.

It is nevertheless advisable for future development the integration of alternative source zonation models in the logic tree. Possible scenarios will be discussed during the next workshop of the project in Pavia.

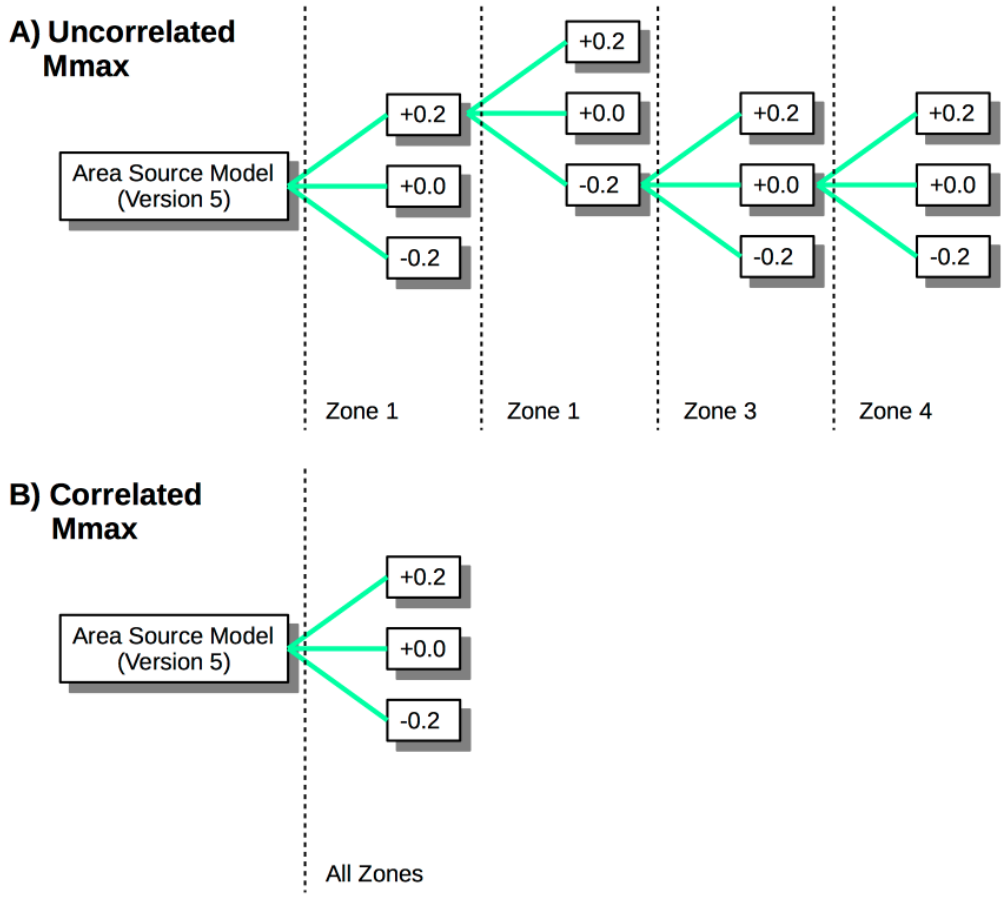

Figure 5.4 – *Schematic representation of the source logic tree structure. Two branching approaches are here shown to model the epistemic variability of maximum magnitude. The first approach is base on multiple branching levels, while the second has only one.*

6. PSHA Results

6.1 Calculation Settings

Hazard computations have been performed using OpenQuake engine (Version 1.10) through the available *classical* calculator for distributed seismicity (see OpenQuake Reference Manual for details on available calculators).

Investigation area consists of a mesh of 2722 sites with 0.5° (about $50Km$) resolution. Such area includes all earthquake source zones described in chapter 3, plus a buffer region of not less than about $100Km$ (with the only exception of the "*horn of Africa*", which was entirely included in the model). For each site of the mesh, free rock conditions are assumed, with a fixed Vs_{30} reference of $600m/s$. Unfortunately, calculation of site-specific hazard is impractical for such a large area. For city scenario, however, it is highly advisable the use of site-specific information from local investigations and microzonation studies. This is a possible second-phase extension of this study.

Target ground motion intensity for calculation is 5% damped response spectral acceleration (in g), estimated for probabilities of exceedance of 10% and 2% within an investigation time of 50 years. This corresponds respectively to return periods of about 2475 and 475 years. Due to the substantial lack of historical records for proper calibration of the large magnitude rates, we avoid using longer return periods (or equivalently too low probability of exceedance).

According to the possibilities of the selected GMPEs, spectral acceleration has been computed at *PGA* and for the response spectral periods of $0.05s$, $0.1s$, $0.2s$, $0.5s$, $1s$ and $2s$. Ground motion integration has been conservatively truncated at 3 *sigma* of the predictions. Output of the calculation are mean and quantile (0.15, 0.5 and 0.85) hazard curves at each site, together with Uniform Hazard Spectra (UHS) and hazard maps, which are described in the next sections.

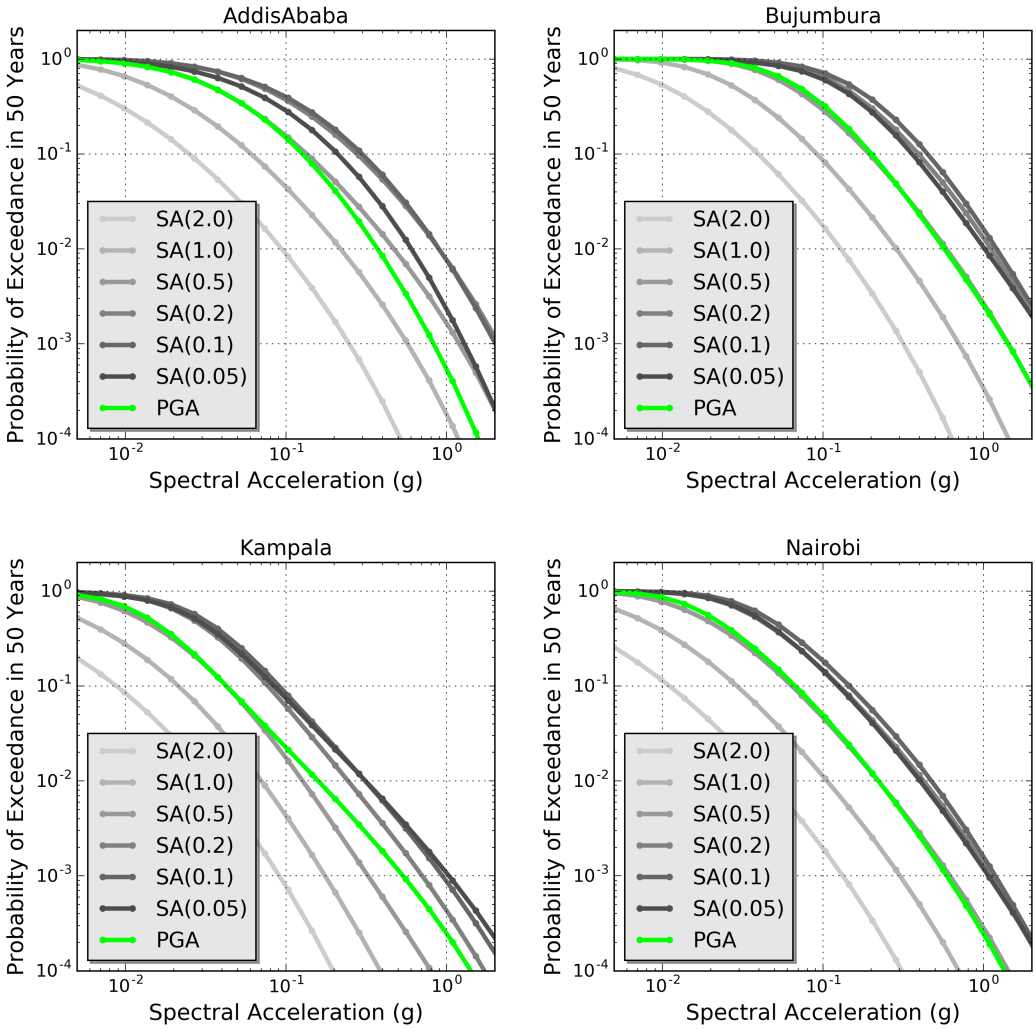

Figure 6.1 – *Mean hazard curves computed at PGA (in green) and at different spectral periods (0.05s to 2s) for four selected African capitals.*

6.2 Calculation Output

Hazard calculations have been performed for each site of the investigation grid. For the sake of conciseness, however, in the following we illustrate hazard curves for four selected African capitals, which are considered of significant for risk analysis:

- Addis Ababa (Ethiopia);
- Kampala (Uganda);
- Nairobi (Kenya);
- Bujumbura (Burundi).

For each examples, hazard curves and uniform hazard spectra are briefly discussed.

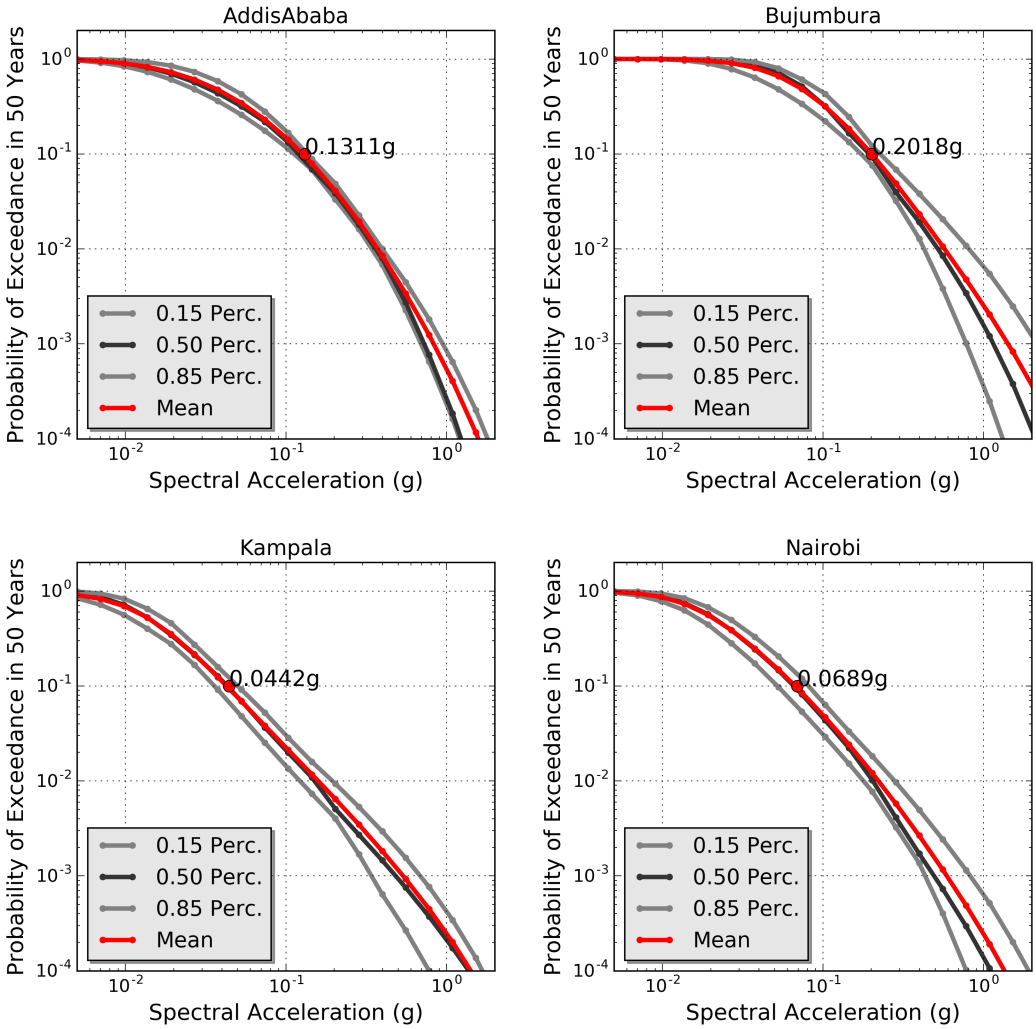

Figure 6.2 – *Mean and quantile hazard curves computed at PGA for four selected African capitals. Spectral acceleration corresponding to 10% probability of exceedance in 50 years is shown with a red dot.*

6.2.1 Earthquake Hazard Curves

Hazard curves are preliminary calculated (see figure 6.1) for fixed response spectral acceleration ordinates between 0.005g and 2.13g and separately for each prescribed spectral period (including PGA). Acceleration corresponding to the target probability of exceedance is subsequently extracted from the curves by linear interpolation. In figure 6.2 are presented mean and quantile hazard curves at PGA for the four example locations. As it can be observed from the plot, logic tree variability is rather small and a good matching between mean and 0.5 quantile estimates is present for probability of exceedance larger than 0.01 (1%).

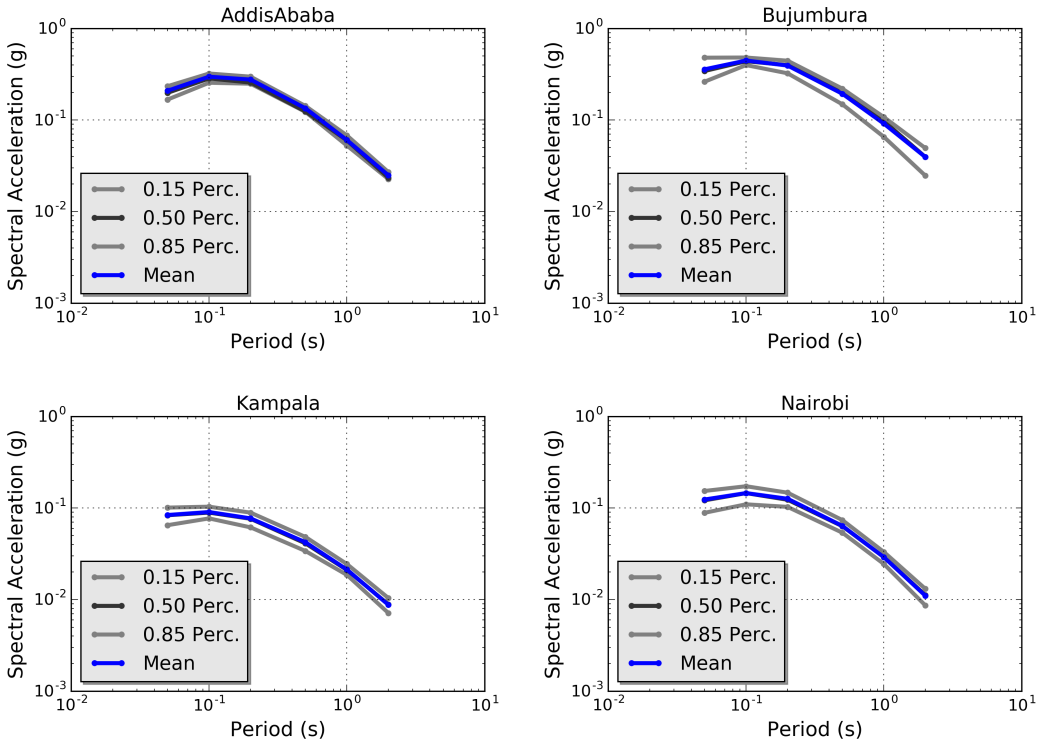

Figure 6.3 – *Mean and quantile Uniform Hazard Spectra computed for the four selected African capitals.*

6.2.2 *Uniform Hazard Spectra*

Uniform Hazard Spectra (UHS) are computed by collecting ground motion for a given probability of exceedance over a spectrum of different response periods. This representation is useful to highlight those periods where larger spectral acceleration is expected. It is however important to stress that UHS cannot be directly used to model local scenarios (e.g. for the selection of a reference earthquake), as the different spectral ordinates might be (and likely are) linked to different controlling events. For that purpose, a disaggregation procedure is best suited.

In figure 6.3 mean and quantile UHS are shown for the four selected African capitals. It is evident a considerable contribution to hazard for periods between $0.1s$ and $0.2s$. This is not surprising as it is related to residual effect of local soil conditions, which are likely to affect ground motion predicted in this frequency band $(5-10Hz)$. Such period range is also significant from engineering perpective, as it match the resonance response of common buildings in urban environments.

6.2.3 *Earthquake Hazard Maps*

A series of hazard maps have been produced for different return periods (see figure 6.4, 6.5, 6.6, 6.7, 6.8, 6.9 and 6.10 for 10% probability of exceedance in 50 years; investigated area is delimited with dashed line). Largest accelerations are found for periods of 0.1s and 0.2s along the eastern branch of the EARS (0.5g), particularly for source zones 06.00 and 08.00. Moderate acceleration (less than 0.35g) is experienced in the Afar region (zone 01.00) in north Ethiopia. South Ethiopia (zone 04.00) presents levels (0.24g at 0.2s) which are comparable to western EARS (zone 15.00) and the side seismic belts of Zambia (zone 12.01). Remaining portions of the rift are affected by lower hazard, with acceleration generally lower than 0.2g.

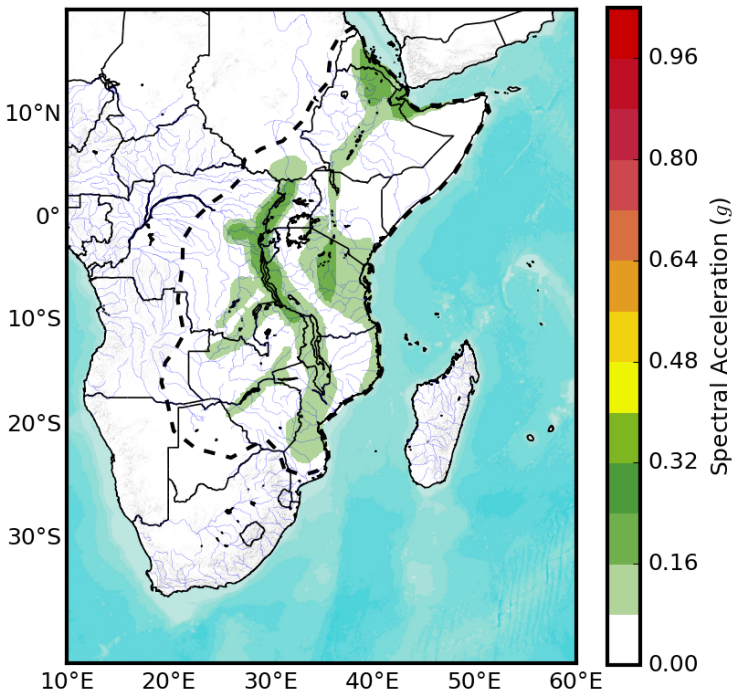

Figure 6.4 – *Map of spectral acceleration at **PGA** for 10% probability of exceedance in 50 years.*

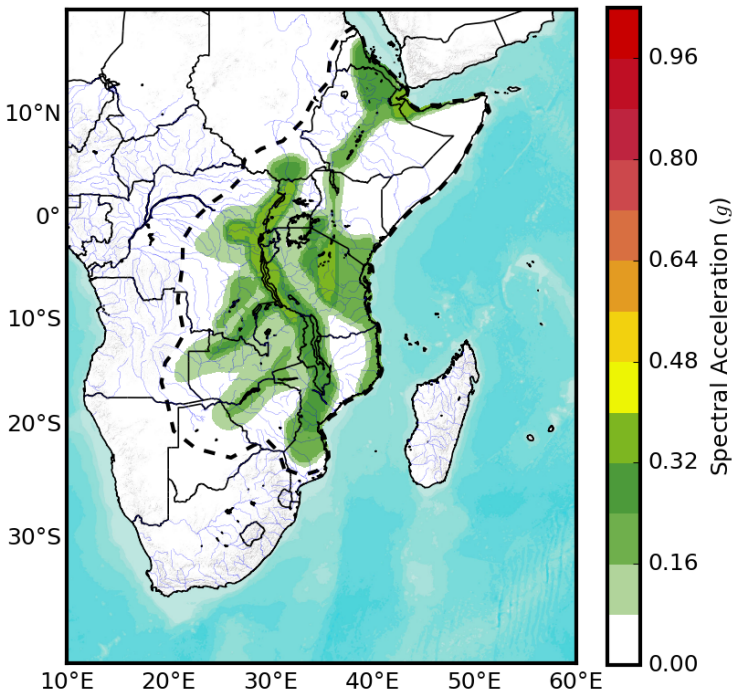

Figure 6.5 – *Map of spectral acceleration at **0.05s** for 10% probability of exceedance in 50 years.*

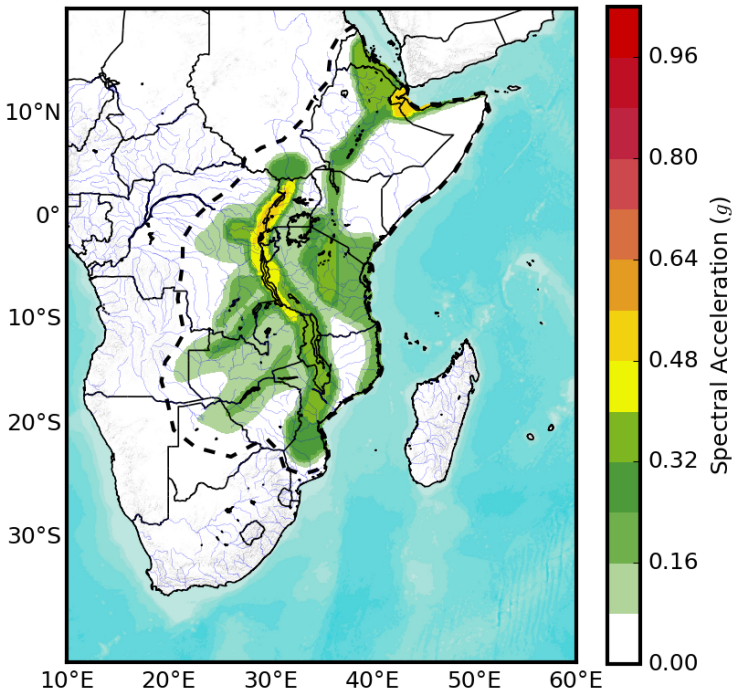

Figure 6.6 – *Map of spectral acceleration at **0.1s** for 10% probability of exceedance in 50 years.*

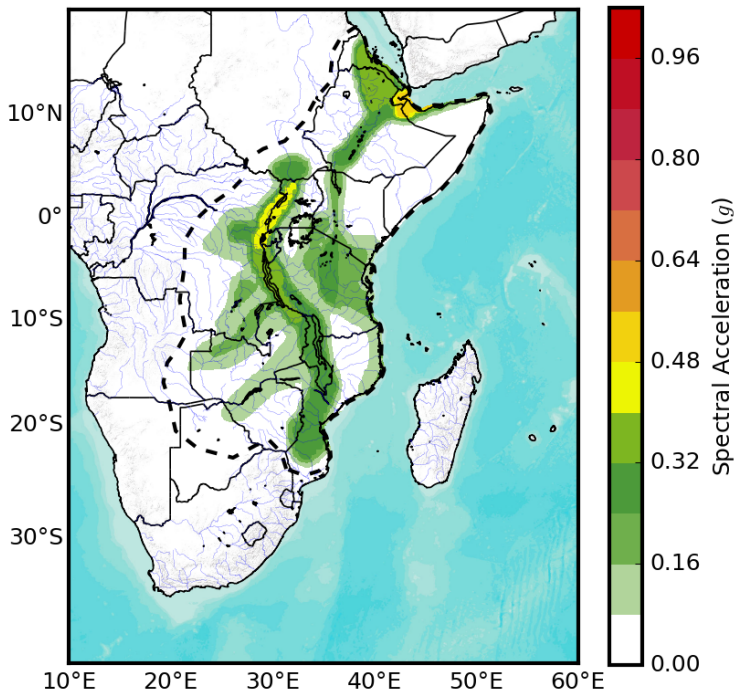

Figure 6.7 – *Map of spectral acceleration at **0.2s** for 10% probability of exceedance in 50 years.*

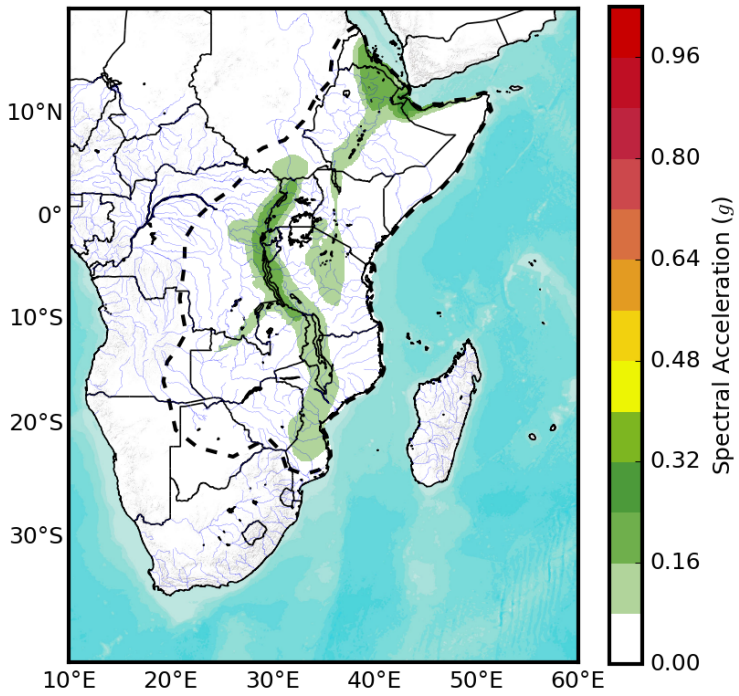

Figure 6.8 – *Map of spectral acceleration at **0.5s** for 10% probability of exceedance in 50 years.*

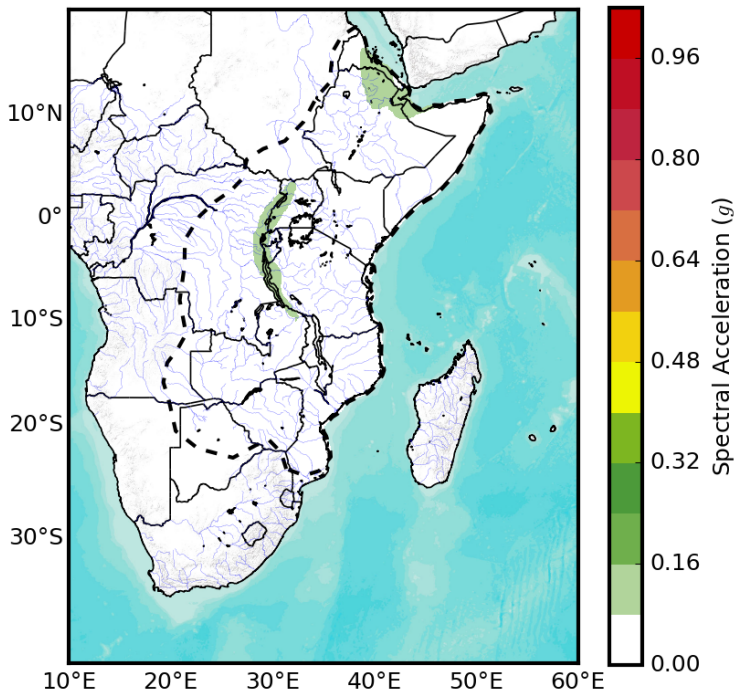

Figure 6.9 – *Map of spectral acceleration at **1.0s** for 10% probability of exceedance in 50 years.*

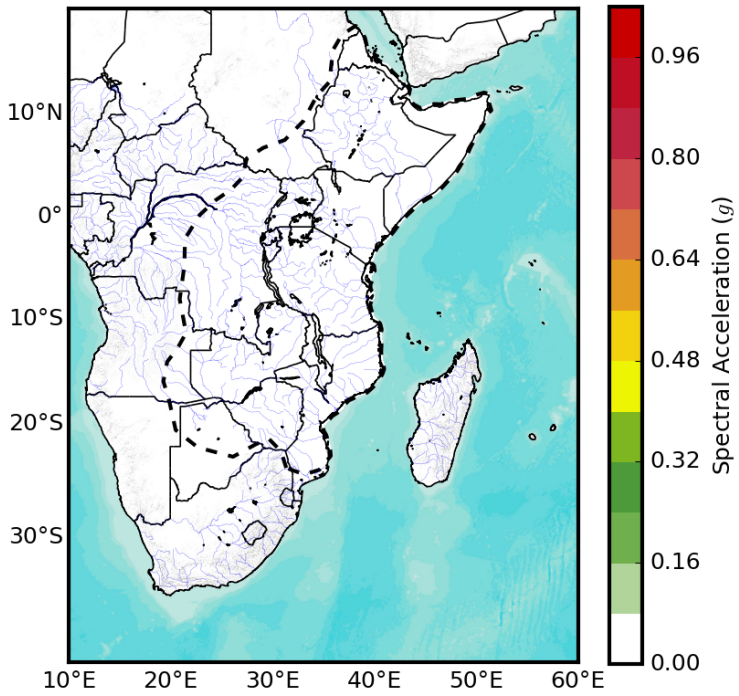

Figure 6.10 – *Map of spectral acceleration at **2.0s** for 10% probability of exceedance in 50 years.*

Acknowledgments

This study is made possible by the generous support of the American people through the United States Agency for International Development (USAID). The contents are the responsibility of GEM and do not necessarily reflect the views of USAID or the United States Government.

Bibliography

Books

Casey, M., C. Ebinger, D. Keir, R. Gloagen, and R. Mohamed (2006). *Strain accomodation in transitional rifts : extension by magma intrusion and faulting in the Ethiopian rift magmatic segment. In: Yirgu, G., Ebinger, C.J., Maguire, P.K.H. (Eds.), The Afar volcanic province within the East African Rift System*. Volume 259. Geol. Soc. Lond. Spec. Publ., pages 143–163 (cited on page 23).

Engdahl, E. and A. Villaseñor (2002). *Global Seismicity: 1900–1999, in W.H.K. Lee, H. Kanamori, P.C. Jennings, and C. Kisslinger (editors), International Handbook of Earthquake and Engineering Seismology, Part A, Chapter 41*. Academic Press, 665–690 (cited on page 17).

Midzi, V., and B. Manzunzu (2014). *Large recorded earthquakes in sub-Saharan Africa. In Extreme Natural Hazards, Disaster Risks and Societal Implications*. Cambridge University Press (cited on page 10).

Articles

Aki, K. (1965). "Maximum likelihood estimate of b in the formula log (N) = a - bM and its confidence limits". In: *Bull. Earthq. Res. Inst. Tokyo Univ.* 43, pages 237–239 (cited on page 30).

Akkar, S., M. Sandikkaya, and J. Bommer (2014). "Empirical ground-motion models for point- and extended-source crustal earthquake scenarios in Europe and the Middle East". In: *Bulletin of Earthquake Engineering* 12, pages 359–387 (cited on page 36).

Ambraseys, N. (1991a). "Earthquake hazard in the Kenya Rift: the Subukia earthquake 1928". In: *Geophysical Journal International* 105, pages 253–269 (cited on page 10).

— (1991b). "The Rukwa earthquake of 13 Dec. 1910 in E. Africa". In: *Terra Nova* 3, pages 203–208 (cited on page 10).

Ambraseys, N. and R. Adams (1991). "Reappraisal of major African earthquakes, south of 20°N, 1900-1930". In: *Natural Hazards* 4, pages 389–419 (cited on page 10).

Atkinson, G. and D. Boore (2006). "Earthquake ground-motion prediction equations for eastern North America". In: *Seismol. Soc. Am.* 96, 2181–2205 (cited on page 36).

Biggs, J., E. Nissen, T. Craig, J. Jackson, and D. Robinson (2010). "Breaking up the hanging wall of a rift-border fault : The 2009 Karonga earthquakes, Malawi". In: *Geophys. Res. Lett.* 37 (cited on page 25).

Biggs, J., N. Amelung, T. Gourmelen, H. Dixon, and S. Kim (2009). "InSAR observations of 2007 Tanzania rifting episode reveal mixed fault and dyke extension in an immature continental rift". In: *Geophys. J. Int.* 179.1, pages 549–538 (cited on page 26).

Boyd, F. and J. Gumey (1986). “Diamonds and the African lithosphere”. In: *Science* 232, pages 472–477 (cited on page 24).

Calais, E., N. d’Oreye, J. Albaric, A. Deschamps, D. Delvaux, J. Deverchere, C. Ebinger, R. W. Ferdinand, F. Kervyn, A. S. Macheyeki, A. Oyen, J. Perrot, E. Saria, B. Smets, D. S. Stamps, and C. Wauthier (2008). “Aseismic strain accommodation by slow slip and dyking in a youthful continental rift, East Africa”. In: *Nature* 456.7223, pages 783–787 (cited on page 26).

Chesley, J., R. Rudnick, and C. Lee (1999). “Re-Ossystematics of mantlexenoliths from the East African Rift: Age, structure, and history of the Tanzanian craton”. In: *Geochim. Cosmochim. Acta* 63, pages 1203–1227 (cited on page 23).

Chiou, B.-J. and R. Youngs (2014). “Update of the Chiou and Youngs NGA Model for the Average Horizontal Component of Peak Ground Motion and Response Spectra”. In: *Earthquake Spectra* 30.3, pages 1117–1153 (cited on page 36).

Chorowicz, J. (2005). “The East African rift system”. In: *Journal of African Earth Sciences* 43, pages 379–410 (cited on page 25).

Craig T.J., J. J. P. K. and D. McKenzie (2011). “Earthquake distribution patterns in Africa: their relationship to variations in lithospheric and geological structure, and their rheological implications”. In: *Geophysical Journal International* 185, pages 403–434 (cited on pages 25, 26).

Dawson, J. (1992). “Neogene tectonics and volcanicity in the North Tanzania sector of the Gregory Rift Valley: Contrasts with the Kenya sector”. In: *Tectonophysics* 204, pages 81–92 (cited on pages 26, 27).

Delvaux, D. and A. Barth (2010a). “African stress pattern from formal inversion of focal mechanism data”. In: *Tectonophysics* 482, pages 105–128 (cited on page 25).

— (2010b). “African stress pattern from formal inversion of focal mechanism data”. In: *Tectonophysics* 482, pages 105–128 (cited on page 27).

Delvaux, D. and M. Hanon (1993). “Neotectonics of the Mbeya area, SW Tanzania”. In: *Mus. Roy. Afr. Centr. Tervuren (Belg.), Dept. Geol. Min. Rapp. Ann.* 991-992, pages 87–97 (cited on page 27).

Delvaux, D., F. Kervyn, A. Macheyeki, and E. Temu (2012). “Geodynamic significance of TRM segment in East African Rift (W-Tanzania): active tectonics and paleostress in the Ufipa plateau and Rukwa basin”. In: *J. Struct. Geol.* 37, pages 161–180 (cited on page 25).

Ebinger, C. J. (1989). “Tectonic development of the Western branch of the East African Rift system”. In: *Geol. Soc. of Am. Bull.* 101, pages 885–993 (cited on page 27).

Edwards, B., B. Allmann, D. Fah, and J. Clinton (2010). “Automatic computation of moment magnitudes for small earthquakes and the scaling of local to moment magnitude”. In: *Geophysical Journal International* 183, 407–420 (cited on pages 17, 18).

Ekström, G., M. Nettles, and A. M. Dziewonski (2012). “The global CMT project 2004-2010: Centroid-moment tensors for 13,017 earthquakes”. In: *Phys. Earth Planet. Inter.* 200-201, pages 1–9 (cited on page 14).

Fenton, C. and J. Bommer (2006). “The Mw 7.0 Machaze Mozambique earthquake of 23 February 2006”. In: *Seismol. Res. Lett.* 77, pages 425–439 (cited on page 27).

Furman, T., J. Kaleta, J. Bryce, and B. Hanan (2006). “Tertiairy mafic lava of Turkana, Kenya: Constraints on EAST African plume structure and the occurrence of high $\mu volcanism in Af rica$”. In: *J. Petro.* 47.6, pages 1221–1244 (cited on pages 10, 26).

Gardner, J. K. and L. Knopoff (1974). “Is the sequence of earthquakes in Southern California, with aftershocks removed, Poissonian?” In: *Bulletin of the Seismological Society of America* 64.5, pages 1363–1367 (cited on page 19).

George, R., N. Rogers, and S. Kelley (1998). “Earliest magmatism in Ethiopia : Evidence for two mantle plumes in one flood basalt province”. In: *Geology* 26, pages 923–926 (cited on page 26).

Green, W., U. Achauer, and R. Meyer (1991). “A three-dimensional seismic image of the crust and upper mantle beneath the Kenya rift”. In: *Nature* 354, 199–203 (cited on page 24).

Grimison, N. and W. P. Chen (1988). “Earthquakes in Davie Ridge-Madagascar region and the southern Nubian-Somalian plate boundary”. In: *J. Geophys. Res.* 93, pages 10439–10450 (cited on page 27).

Gurnis, M., J. Mittovica, J. Ritsema, and H. Van Hest (2000). “Constraining mantle density structure using geological evidence of surface uplift rates: The case of African superplume”. In: *Geochem. Geophys. Geosyst.* 1, page 10220 (cited on page 10).

Hartnady, C. (1990). “Seismicity and plate boundary evolution in Southeastern Africa”. In: *S. Afr. J. Sci.* 93, pages 473–484 (cited on page 27).

— (2002). “Earthquake hazard in Africa: perspectives on the Nubia-Somalia boundary”. In: *S. Afri. J. Sci.* 98, pages 425–428 (cited on page 23).

— (2006). “Seismotectonics of Southern Mozambique”. In: *Paper presented at 21st Colloquium on African Geology (CAGE21).Geol. Soc. Of Sci. Afr., Maputo, Mozambique* (cited on page 27).

Hartnady, C., H. Ben-Avrahan, and J. Rogers (1992). “Deep-ocean basin basins and submarine rises of the continental margin of south-eastern Africa: New geological research”. In: *S. Afr. J. Sci* 88, pages 534–539 (cited on page 27).

Kebede, F. and O. Kulhanek (1991). “Recent seismicity of the East African rift system and its implications”. In: *Phys. Earth. Planet. Inter.* 68, pages 259–273 (cited on page 22).

Keir, D., J. Hamling, A. Ayele, E. Calais, and T. Wright (2009). “Evisence for focused magmatic accretion at segment centers from lateral dike injection captured beneath the Red Sea Rift in Afar”. In: *Geology* 37, pages 59–62 (cited on page 23).

Le Gall, B., L. Gernignon, J. Rolet, C. Ebinger, R. Gloageri, O. Nilsen, H. Dypvik, B. Derffontaines, and A. Mruma (2004). “Neogene-Recent rift propagation in Central Tanzania: Morphostructural and aeromagnetic evidence from the Kilombero area”. In: *Geol. Soc. Am. Bull.* 116, pages 490–510 (cited on page 26).

Le Gall, B., P. Nonnotte, J. Rolet, M. Benoit, H. Guillou, M. Mousseau-Nonnotte, J. Albaric, and J. Devechere (2008). “Rift propagation at craton margin. Distribution of faulting

and volcanism in the North Tanzania Divergence: (East Africa) during Neogene times". In: *Tectonophysics* 448, pages 1–19 (cited on page 27).

Lithgow-Berteloni, C. and P. Silveri (1998). "Dynamic topography, plate driving forces and the African superswell". In: *Nature* 395, pages 269–272 (cited on page 10).

Lyons, R., C. Scholz, M. Buoniconti, and M. Martin (2011). "Late quaternary stratigraphy pf the Lake Malawi Rift, East Africa. An integration of drill-core and seismic resection data". In: *Paleogeogr. Paleoclimatol. Paleoecol.* 303, pages 20–37 (cited on pages 10, 25).

MacGregor, D. (2015). "History of the development of the East African Rift System: A series of interpreted maps through time". In: *Journal of African Earth Sciences* 101, pages 232–252 (cited on pages 21, 23, 29, 30).

Macheyeki, A., D. Delvaux, M. Debatist, and M. Mruma (2008). "Fault kinematic s and tectonic stress in the seismically active Manyara-Dodoma Rift segment in Central Tanzania: implications for the East African Rift". In: *J. Afr. Earth Sci.* 51, pages 165–188 (cited on page 26).

McDougall, I. and F. Brown (2009). "Timing of volcanism and evolution of northern Kenya Rift". In: *Geol. Mag.* 146.1, pages 34–47 (cited on page 26).

Mignan, A. and J. Woessner (2012). "Estimating the magnitude of completeness for earthquake catalogs". In: *Community Online Resource for Statistical Seismicity Analysis* (cited on page 31).

Mougenot, D., M. Recq, P. Virlogeux, and C. Lepvrier (1986). "Seaward extension of the East African Rift". In: *Nature* 321, pages 599–603 (cited on page 27).

Nyblade, A. and S. Robinson (1994). "The African superswel". In: *Geophys. Res. Lett.* 21.9, pages 765–768 (cited on page 10).

Pezeshk S., Z. A. and B. Tavakoli (2011). "Hybrid Empirical Ground-Motion Prediction Equations for Eastern North America Using NGA Models and Updated Seismological Parameters". In: *Bull Seism. Soc. Am.* 101.4, pages 1859–1870 (cited on page 36).

Pik, R., B. Marty, J. Carignan, and J. Lave (2003). "Stability of the upper Nile drainage network (Ethiopia) deduced from (U-Th)/He thermochronometry : implication for uplift and erosion of the Afar plume dome". In: *Earth. Planet. Sci. Lett.* 215, pages 73–88 (cited on page 10).

Pik, R., B. Marty, and D. Hilton (2006). "How many mantle plumes in Africa? The geochemical point of view". In: *Chem. Geol.* 226, pages 100–114 (cited on page 26).

Rasskazov, S., N. Logatchev, A. Ivanov, A. Boveri, M. Maslovsskaya, E. Saranina, I. Brandt, and S. Brandt (2003). "A magmatic episode in the Western Rift of East Africa". In: *Geol. Geofiz.* 44, pages 317–324 (cited on page 27).

Ritsema, J., H. Van hest, and J. Woodhouse (1998). "Complex shear wave velocity structure imaged beneath Africa and Iceland". In: *Science* 286, pages 1925–1928 (cited on pages 10, 24).

Roberts, E., N. Stevens, P. O'Connor, P. Dirks, M. Gottfried, W. Clyde, R. Armstrong, A. Kemp, and S. Hemming (2012). "Initiation of the Western Branch of the East African Rift, coeval with the eastern Branch". In: *Nat. Geosc.* 5.4, pages 289–294 (cited on page 25).

Rydelek, P. A. and I. S. Sacks (1989). "Testing the completeness of earthquake catalogs and the hypothesis of self-similarity". In: *Nature* 337, 251–253 (cited on page 31).

Saria, E., E. Calais, D. S. Stamps, D. Delvaux, and C. Hartnady (2014). "Present-day kinematics of the East African Rift". In: *J. Geophys. Res. Solid Earth* 119, 3584–3600 (cited on pages 21, 23).

Shudofsky, G. (1985). "Source mechanisms and focal depths of East African earthquakes using the Rayleigh-wave inversion and body-wave modelling". In: *Geophys. J. R., Astr.Soc.* 83, pages 563–634 (cited on page 22).

T., M. (2007). "Some characteristics of aftershock sequences of major earthquakes from 1994 to 2002 in the Kivu Province, Western Rift Valley of Africa". In: *Tectonophysics* 439, pages 1–12 (cited on page 26).

Tanaka K., S. H. T. S. and N. Zana (1980). "The Earthquake Generating Stress in the Western Rift Vaklley of Africa". In: *J. Phys. Earth* 28, pages 45–57 (cited on page 25).

Uhrhammer, R. (1986). "Characteristics of northern and central California seismicity". In: *Earthquake Notes* 57.1, page 21 (cited on page 19).

Vilanova, S., E. Nemser, G. Besana-Ostman, M. Bezzeghoud, J. F. Borges, A. da Silveira, J. Cabral, J. Carvalho, P. Cunha, R. Dias, J. Madeira, F. Lopes, C. Oliveira, H. Perea, J. García-Mayordomo, I. Wong, R. Arvidsson, and J. Fonseca (2014). "Incorporating descriptive metadata into seismic source zone models for Seismic-Hazard Assessment: a case study of the Azores–West Iberian region". In: *Bulletin of the Seismological Society of America* 104, pages 1212–1229 (cited on page 21).

Vittori, E., D. Delvaux, and F. Kervyn (1997). "Kanda fault: a major seismogenic element west of the Rukwa Rift (East Africa: Tanzania)". In: *J. Geophys.* 24.1-4, pages 139–153 (cited on page 25).

Weatherill, G. A., M. Pagani, and J. Garcia (2016). "Exploring earthquake databases for the creation of magnitude-homogeneous catalogues: tools for application on a regional and global scale". In: *Geophys. J. Int.* 206.3, pages 1652–1676 (cited on page 17).

Weeraratne, D., D. Forsyth, K. Fisher, and A. Nyblade (2003). "Evidence for an upper mantle plume beneath the Tanzanian Craton from Rayleigh-wave tomography". In: *J. Geophys. Res.* 108.89, page 2427 (cited on page 24).

Weichert, D. H. (1980). "Estimation of the earthquake recurrance parameters for unequalobservation periods for different magnitudes". In: *Bulletin of the Seismological Society of America* 70.4, 1337–1346 (cited on page 31).

Wendlandt, R. and P. Morgan (1982). "Lithosphere thinning associated with rifting in East Africa". In: *Nature* 298, pages 734–736 (cited on page 24).

Woessner, J. and S. Wiemer (2005). “Assessing the quality of earthquake catalogues: Estimating the magnitude of completeness and its uncertainty”. In: *Bull. Seismol. Soc. Am.* 95, 684–698 (cited on page 31).

Wolfenden, E., C. Ebinger, G. Yiirgu, A. Deino, and D. Ayalew (2004). “Evolution of the northern Main Ethiopian Rift: Birth of a triple junction”. In: *Earth Planet. Sci.* (Cited on page 23).

Worku, A. (2014). “The status of basic design ground motion provisions in seismic design codes of Sub-Saharan African countries”. In: *Journal of the South African Institution of Civil Engineering* 56, pages 40–53 (cited on page 8).

Yang, Z. and W. P. Chen (2010). “Earthquakes along the East African Rift System: a multiscale, system-wide perspective”. In: *Journal of Geophysical Research* 115, B12309 (cited on pages 25–27).

Zana, N. (1977). “The Seismicity of the Western Rift Valley of Africa and associated problems”. In: *Doctorate Thesis, Tohoku University, Sendai, Japan*, 177 pp (cited on page 25).

Zana, N. and H. Hamaguchi (1978). “Some characteristics of aftershock sequences in the Western RiftValley of Africa”. In: *Tohoku Geophys. Journ. (Sci. Rep. Tohoku Univ., Ver.5), Geophysics* 25.2, pages 55–72 (cited on page 25).

Zana, N., M. Wafula, N. Lukaya, and M. Batabolo (2004). “The Kabalo earthquake in D. R. Congo on September 11, 1992: Field observations and damages Quelques résultats de Recherches en Géophysique”. In: *Centre de Recherches et Pedagogie appliqués (C. R. P. A), I. P.N, Kinshasa*, pages 77–89 (cited on page 26).

Other Sources

MWK (1973). *Code of Practice – Earthquake Design for Kenya. Nairobi*. Technical report. Ministry of Works of Kenya (cited on page 8).

MWUD (1995). *EBCS 8: Design of Structures for Earthquake Resistance. Addis Ababa*. Technical report. Ministry of Works and Urban Development of Ethiopia (cited on page 9).

Stepp, J. C. (1971). *An investigation of earthquake risk in the Puget Sound area by use of the type I distribution of largest extremes*. Technical report. PhD thesis, Pennsylvania State University (cited on page 32).

UNBS (2003). *US 319:2003: Seismic Code of Practice for Structural Designs. Kampala, Uganda*. Technical report. Uganda National Bureau of Standards (cited on page 9).

Van Stiphout, T., J. Zhuang, and D. Marsan (2012). *Theme V - Models and techniques for analysing seismicity*. Technical report. Community Online Resource for Statistical Seismicity Analysis. url: http://www.corssa.org (cited on page 19).